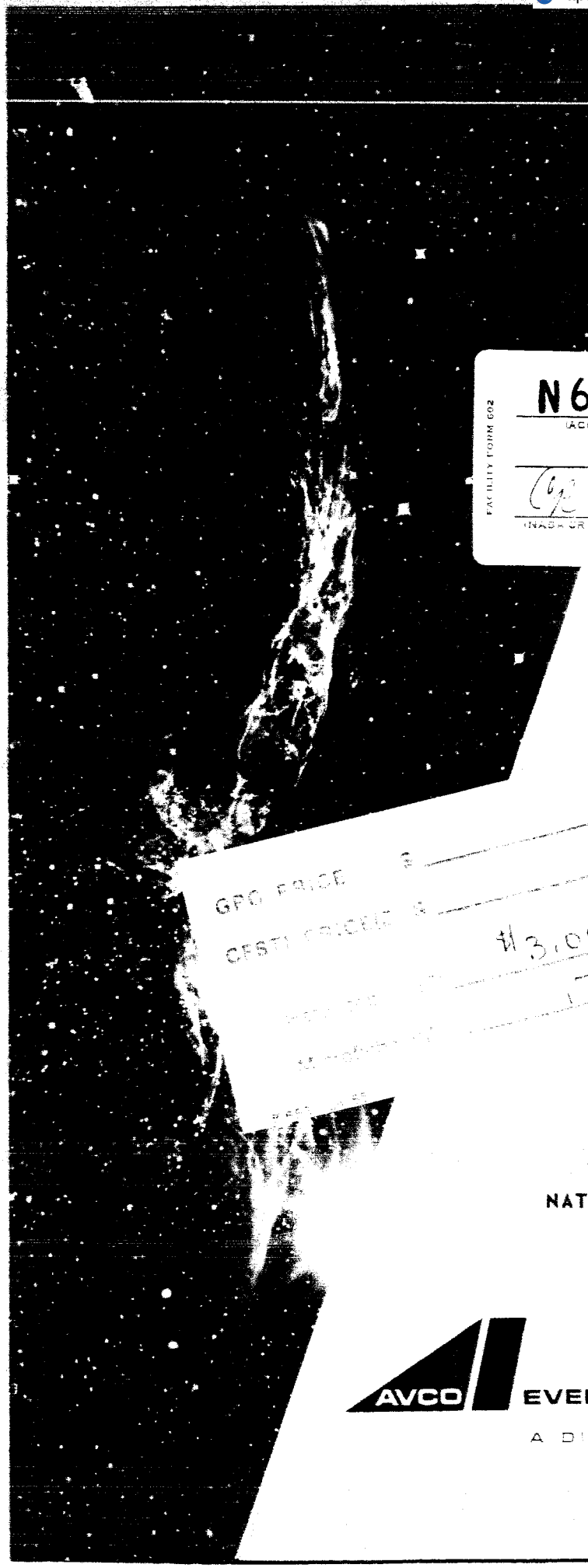

EXPERIMENTAL INVESTIGATION OF ADVANCED SUPERCONDUCTING MAGNETS

Ethan Hoag

ANNUAL REPORT

Contract No. NAS 8-5279

July 1966

prepared for

GEORGE C. MARSHALL SPACE FLIGHT CENTER

NATIONAL AERONAUTICS AND SPACE ADMINISTRATION

Huntsville, Alabama

AVCO EVERETT RESEARCH LABORATORY

A DIVISION OF AVCO CORPORATION

EXPERIMENTAL INVESTIGATION OF ADVANCED SUPERCONDUCTING MAGNETS

by

Ethan Hoag

ANNUAL REPORT

AVCO EVERETT RESEARCH LABORATORY
a division of
AVCO CORPORATION
Everett, Massachusetts

Contract No. NAS 8-5279

July 1966

prepared for

GEORGE C. MARSHALL SPACE FLIGHT CENTER
NATIONAL AERONAUTICS AND SPACE ADMINISTRATION
Huntsville, Alabama

TABLE OF CONTENTS

		Page
I.	TWO DIMENSIONAL EFFECTS IN COMPOSITE CONDUCTORS	1
II.	CURRENT DISTRIBUTION IN SUPERCONDUCTING NB-ZR STRIP	9
III.	OPERATION OF A FACE COOLED NB-ZR STRIP MAGNET	17
IV.	OPERATION OF SUPERCONDUCTORS AT TEMPERATURES BELOW THE LAMBDA POINT	25
V.	BOILING HEAT TRANSFER TO LIQUID HELIUM IN VERTICAL PASSAGES	31
VI.	A COMPARATIVE ANALYSIS OF SUPERCONDUCTING MAGNET ENERGIZING SYSTEMS	39
VII.	OPERATION OF AN EXPERIMENTAL TRANSFORMER TYPE ENERGIZER	69
	REFERENCES	78

I. TWO DIMENSIONAL EFFECTS IN COMPOSITE CONDUCTORS

Consider a composite conductor consisting of a superconductor in good thermal and electrical contact with a normal conductor, and in which some or all of the conductor perimeter is in contact with a liquid helium bath at temperature T_b.

$$- \frac{\partial}{\partial x} \left(kA \frac{\partial T}{\partial x}\right) + hp\,(T - T_b) = v \cdot I \tag{1}$$

where x is the direction along the conductor, A is the cross-sectional area, p is the wetted perimeter, k is the thermal conductivity of the normal material and h is the heat transfer coefficient between the conductor and the liquid helium bath.

The voltage per unit length v is given by:

$$v = \frac{\rho}{A} f I \qquad 0 \leq f \leq 1.0 \tag{2}$$

The amount of current the superconductor will carry is determined by its temperature and the magnetic field to which it is exposed. If we assume for simplicity that the superconductor current decreases linearly with increasing temperature then:

$$I_s = I_c \left(1 - \frac{T - T_b}{T_c - T_b}\right) \tag{3}$$

where I_c is the critical current at the external magnetic field at the bath temperature. The critical temperature T_c is the critical temperature with no current in the superconductor in the presence of the applied magnetic field. The quantity f is given by:

$$f = I - \frac{I_s}{I} = 1 - \frac{I_c}{I} \left(1 - \frac{T - T_b}{T_c - T_b}\right) \tag{4}$$

making use of Eqs. (2) and (4), Eq. (1) can be put in the following forms:

$$\left.\begin{matrix} f = 0 \\ v = 0 \end{matrix}\right\} \frac{d^2\theta}{d\zeta^2} - \theta = 0 \qquad \begin{matrix} \text{All current in} \\ \text{the superconductor} \end{matrix} \tag{5}$$

$0 < f < 1.0$, $v = \frac{\rho}{A} If$: $\frac{d^2\theta}{d\zeta^2} - \theta(1 - a\tau) - a\tau(1 - \tau) = 0$ — Current shared between the superconductor and normal conductor (6)

$f = 1.0$, $v = \frac{\rho}{A} If$: $\frac{d^2\theta}{d\zeta^2} - \theta + a\tau^2 = 0$ — All current in the normal conductor (7)

where the following dimensionless variables have been introduced:

$$\theta = \frac{T - T_b}{T_c - T_b}$$

$$\zeta = \frac{x}{x_o}, \quad x_o = \sqrt{\frac{kA}{hP}}$$

$$\tau = \frac{I}{I_c}$$

$$a = \frac{\rho I_c^2}{h PA (T_c - T_b)}$$

These equations have the following solutions:

$$f = 0, \ v = 0 \qquad \theta = C_1 e\zeta + C_2 e^{-\zeta} \tag{8}$$

$0 < f < 1.0$, $v = \frac{\rho If}{A}$:

$$C_3 \cosh \sqrt{1 - a\tau}\,\zeta + C_4 \sinh \sqrt{1 - a\tau}\,\zeta - \frac{a\tau(1 - \tau)}{1 - a\tau} = \theta \quad \text{for } a\tau < 1.0$$

$$c'_3 \cos \sqrt{a\tau - 1}\,\zeta + c'_4 \sin \sqrt{1 - a\tau}\,\zeta - \frac{a\tau(1 - \tau)}{1 - a\tau} = \theta \quad \text{for } a\tau < 1.0 \tag{9}$$

$$f = 1.0 \qquad \theta = c_5 e^{\zeta} + c_6 e^{-\zeta} + a\tau^2 \tag{10}$$

Equations (8), (9), and (10) can be solved for a variety of different conditions. In this report we shall consider two cases:

a) A small localized heat source

b) A contact

Small Localized Heat Source

Consider the case of a conductor of infinite extent in both directions having a point heat source of power q_h at the origin. The temperature distribution will be symmetrical about the origin and therefore $q_h/2$ will flow in each direction. The boundary conditions at the origin is therefore:

$$q_h/2 = - k A \left.\frac{dT}{dx}\right]_{x = 0} \tag{11}$$

in dimensionless form this reduces to:

$$\left.\frac{d\theta}{d\zeta}\right]_{\zeta = 0} = - \frac{q_h}{2\sqrt{hPkA}\,(T_c - T_b)} = - Q_h \tag{12}$$

To understand the behavior of the superconductor and its normal substrate we need consider only those situations where $f > 0$, since for $f = 0$ all the current flows in the superconductor and we have only a simple steady state heat conduction problem.

We need two solutions - the first one for the case where only part of the current has been driven out of the superconductor at the origin, and the second one for the case where all the current is in the normal conductor at the origin.

Current Shared at the Origin

The solution for this case is broken down into two regions. A region of current sharing which extends a distance $\Delta\zeta$ from the origin and a region in which the temperature decays but all the current is in the superconductor. At the boundary of the two regions the temperature as well as its first derivative are continuous. The temperature at this boundary is such that $f = 0$, therefore the value of θ can be obtained from Eq. (4) as

$$\left.\theta\right]_{\zeta = \Delta\zeta} = 1 - \tau \tag{13}$$

The boundary conditions at $\zeta \rightarrow \infty$ is $\theta \rightarrow 0$.

Using the above boundary conditions the solution is for $a\tau < 1.0$:

$$0 \leq \zeta \leq \Delta\zeta$$

$$\theta = c_3 \cosh \sqrt{1 - a\tau}\,\zeta + c_4 \sinh \sqrt{1 - a\tau}\,\zeta - \frac{a\tau\,(1-\tau)}{1 - a\tau} \qquad (14)$$

$$\Delta\zeta \leq \zeta$$

$$\theta = (1 - \tau)\, e^{-(\zeta - \Delta\zeta)} \qquad (15)$$

where

$$c_3 = \left[\left(\frac{1-\tau}{1-a\tau}\right) + \frac{Q_h}{\sqrt{1-a\tau}} \sinh \sqrt{1-a\tau}\,\Delta\zeta\right]\left[\cosh \sqrt{1-a\tau}\,\Delta\zeta\right]^{-1}$$

$$c_4 = -\frac{Q_h}{\sqrt{1-a\tau}}$$

and the value of $\Delta\zeta$ is obtained from:

$$\left(\frac{1-\tau}{1-a\tau}\right) \tanh \sqrt{1-a\tau}\;\Delta\zeta + \frac{1-\tau}{\sqrt{1-a\tau}} = \frac{Q_h}{\sqrt{1-a\tau}\;\cosh \sqrt{1-a\tau}\;\Delta\zeta} \qquad (16)$$

The solution for $a\tau > 1.0$ is:

$$0 \leq \zeta \leq \Delta\zeta$$

$$\theta = c_3' \cos \sqrt{a\tau - 1}\;\zeta + c_4' \sin \sqrt{a\tau - 1}\;\zeta - \frac{a\tau\,(1-\tau)}{1 - a\tau} \qquad (17)$$

$$\zeta \geq \Delta\zeta$$

$$\theta = (1 - \tau)\, e^{-(\zeta - \Delta\zeta)} \qquad (18)$$

where

$$c'_3 = \left[\left(\frac{1-\tau}{1-a\tau}\right) + \frac{Q_h}{\sqrt{a\tau-1}} \sin\sqrt{a\tau-1}\,\Delta\zeta\right] \Big/ \cos\sqrt{a\tau-1}\,\Delta\zeta \qquad (19)$$

$$c'_4 = -\frac{Q_h}{\sqrt{a\tau-1}}$$

and the value of $\Delta\zeta$ is obtained from:

$$\frac{1-\tau}{1-a\tau} \tan\sqrt{a\tau-1}\,\Delta\zeta - \frac{1-\tau}{\sqrt{a\tau-1}} = -\frac{Q_h}{\sqrt{a\tau-1}\cos\sqrt{a\tau-1}\,\Delta\zeta} \qquad (20)$$

The voltage measured across the conductor from $-\infty$ to $+\infty$ is:

$$V = \int_{-\infty}^{+\infty} v\,a\,x = \frac{2\rho}{A} I x_o \int_o^{\Delta\zeta} f\,a\,\zeta$$

Using Eq. 4 to eliminate f in terms of θ, and performing the indicated integration results in:

$$v = \frac{VA}{2\rho I x_o} = \frac{Q_h - (1+\Delta\zeta)(1-\tau)}{1-a\tau} \qquad (21)$$

This expression for v is good for all values of $a\tau$.

Current all in the Normal Conductor at the Origin

If Q_h is high enough, then all the current will be expelled from the superconductor at the origin, and the temperature distribution has three regions.

The only new boundary is that between region I and II and since f = 1.0 at this boundary, from Eq. 4 the value of θ = 1.0 is obtained.

The solution for $a\tau < 1.0$ is:

$$0 \le \zeta \le \zeta_1$$

$$\theta > c_1 e^{\zeta} + c_2 e^{-\zeta} + a\tau^2 \qquad (22)$$

$$\theta = c_3 \cosh\sqrt{1 - a\tau}\ (\zeta - \zeta_1) + c_4 \sinh\sqrt{1 - a\tau}\ (\zeta - \zeta_1) - \frac{a\tau\,(1 - \tau)}{1 - a\tau} \quad (23)$$

$$\zeta_1 + \Delta\zeta \leq \zeta$$

$$\theta = (1 - \tau)\, e^{-(\zeta - \zeta_1 - \Delta\zeta)} \quad (24)$$

where

$$c_1 = c_2 - Q_h$$

$$c_2 = \frac{1 - a\tau^2 + Q_h e^{\zeta_1}}{e^{\zeta_1} + e^{-\zeta_1}}$$

$$c_3 = \frac{1 - a\tau^2}{1 - a\tau}$$

$$c_4 = \left[(1 - a\tau^2)\tanh\zeta_1 - \frac{Q_h}{\cosh\zeta_1}\right] \Big/ \sqrt{1 - a\tau}$$

and the value of ζ_1 and $\Delta\zeta$ are obtained from:

$$\cosh\sqrt{1 - a\tau}\ \Delta\zeta + \sqrt{1 - a\tau}\sinh\sqrt{1 - a\tau}\ \Delta\zeta = \frac{1 - a\tau^2}{1 - \tau} \quad (25)$$

$$\frac{(1 - a\tau^2)\tanh\zeta_1 - \dfrac{Q_h}{\cosh\zeta_1}}{1 - a\tau} = -\frac{\dfrac{1 - \tau}{1 - a\tau} + \dfrac{1 - a\tau^2}{1 - a\tau}\sinh\sqrt{1 - a\tau}\,\Delta\zeta}{\cosh\sqrt{1 - a\tau}\,\Delta\zeta} \quad (26)$$

Rather than solve explicityly for the solution for $a\tau > 1.0$ it can be obtained directly from the solution for $a\tau < 1.0$ by substituting $i\sqrt{a\tau - 1}$ for $\sqrt{1 - a\tau}$ and performing the necessary simplifications. The results for $a\tau > 1.0$ are:

$$0 \leq \zeta \leq \zeta_1$$

$$\theta = c_1 e^{\zeta} + c_2 e^{-\zeta} + a\tau^2$$

$$\zeta_1 \leq \zeta \leq \zeta_1 + \Delta\zeta$$

$$\theta = c_3 \cos\sqrt{a\tau - 1}\ (\zeta - \zeta) + c_4' \sin\sqrt{a\tau - 1}\ (\zeta - \zeta_1) - \frac{a\tau\,(1 - \tau)}{1 - a\tau}$$

$$\zeta + \Delta\zeta \leq \zeta$$

$$\theta = (1 - \tau)\, e^{-(\zeta - \zeta - \Delta\zeta)}$$

where

$$c_1 = c_2 - Q_h$$

$$c_2 = \frac{1 - a\tau^2 + Q_h e^{\zeta_1}}{e^{\zeta_1} + e^{-\zeta_1}}$$

$$c_3' = \frac{1 - a\tau^2}{1 - a\tau}$$

$$c_4' = (1 - a\tau^2)\tanh\zeta_1 - \frac{Q_h}{\cosh\zeta_1} \Big/ \sqrt{a\tau - 1}$$

and the value of ζ and $\Delta\zeta$ are obtained from:

$$\cos\sqrt{a\tau - 1}\ \Delta\zeta - \sqrt{a\tau - 1}\ \sin\sqrt{a\tau - 1}\ \Delta\zeta = \frac{1 - a\tau^2}{1 - \tau}$$

and:

$$\frac{(1 - a\tau^2)\tanh\zeta_1 - \frac{Q_h}{\cosh\zeta_1}}{\sqrt{a\tau - 1}} = -\frac{\sqrt{\frac{1 - \tau}{a\tau - 1}} - \frac{1 - a\tau^2}{1 - a\tau}\sin\sqrt{a\tau - 1}\,\Delta\zeta}{\cos\sqrt{a\tau - 1}\ \Delta\zeta}$$

The voltage across the conductor from $-\infty$ to $+\infty$ is:

$$V\int_{-\infty}^{+\infty} v\, d\, x = 2\int_{o}^{\zeta_1 + \Delta\zeta} \frac{\rho\, I\, f}{A}\, d_x = \frac{2\rho\, I\, x_o}{A}\left[\int_{o}^{\zeta_1} d\zeta + \int_{\zeta_1}^{\Delta\zeta} f d\zeta\right]$$

substituting for f from Eq. (4) and using the expression for θ the voltage is:

$$v = \frac{VA}{2\rho I x_o} = \tau \zeta_1 - \frac{(1-\tau)(1+\Delta\zeta)}{1-a\tau} - \frac{(1-a\tau^2)\tanh\zeta_1 - \frac{Q_h}{\cosh\zeta_1}}{1-a\tau}$$

This expression for v is valid for all values of $a\tau$. It is currently being evaluated for typical values of $a\tau$ and the other parameters but the results are not as yet available. When completed they will be used to correlate the results of an experiment now underway to actually measure the voltage appearing across a test sample.

II. CURRENT DISTRIBUTION IN SUPERCONDUCTING NB-ZR STRIP

The study of the current density distribution in superconducting strip has been continued in an effort to obtain more quantitative results than those revealed by earlier optical studies.[1] Measurements of the magnetic field at the surface of a current carrying strip have been obtained by scanning across the sample with a very small Hall detector. A computer code has been compiled to analyze the resulting field profiles in order to obtain the current density distribution in the strip.

Experimental Apparatus and Sample

The sample consisted of optimally annealed[2] Nb-25% Zr strip .051 mm thick by 8.34 mm wide soldered to a copper substrate to stabilize it. It was constructed in the form of a closed superconducting loop and energized by means of a DC transformer. In this way, currents up to 3600 A could be generated in the sample with virtually none of the ripple and other noise attendant with a high current external supply.

The physical arrangement is shown in Fig. 1 where the scanning apparatus and the Hall detector are shown mounted on the sample. The detector was a commercially available unit made to our specifications and consisted of a thin wafer of mylar with a bismuth film vacuum deposited in a four terminal Hall configuration. It had an active region 0.5 mm square resulting in an observed resolution of approximately 0.1 mm.

A photograph of the scanning apparatus is shown in Fig. 2. It consisted of a small worm drive taken from a trimmer potentiometer and modified. The worm was driven by means of a shaft from outside the dewar and the position was sensed by means of a potentiometer driven by it through a reduction gear.

Data was taken in the form of magnetic field profiles obtained with the help of an X-Y recorder.

In general, the procedure was to take field profile scans while holding the field and/or transport current fixed at various values, the main aim being to learn how the current density spreads throughout the superconductor as changes are made in these quantities. After thoroughly exploring a stabilized sample in this manner, it was delaminated in the test region and explored again so that a comparison could be obtained between stabilized and unstabilized operation. In all cases a heater was provided which could raise the temperature of the entire scanned region above the critical temperature so that trapped current distributions could be removed at will.

Using the sample in its stabilized state the following series of scans was performed.

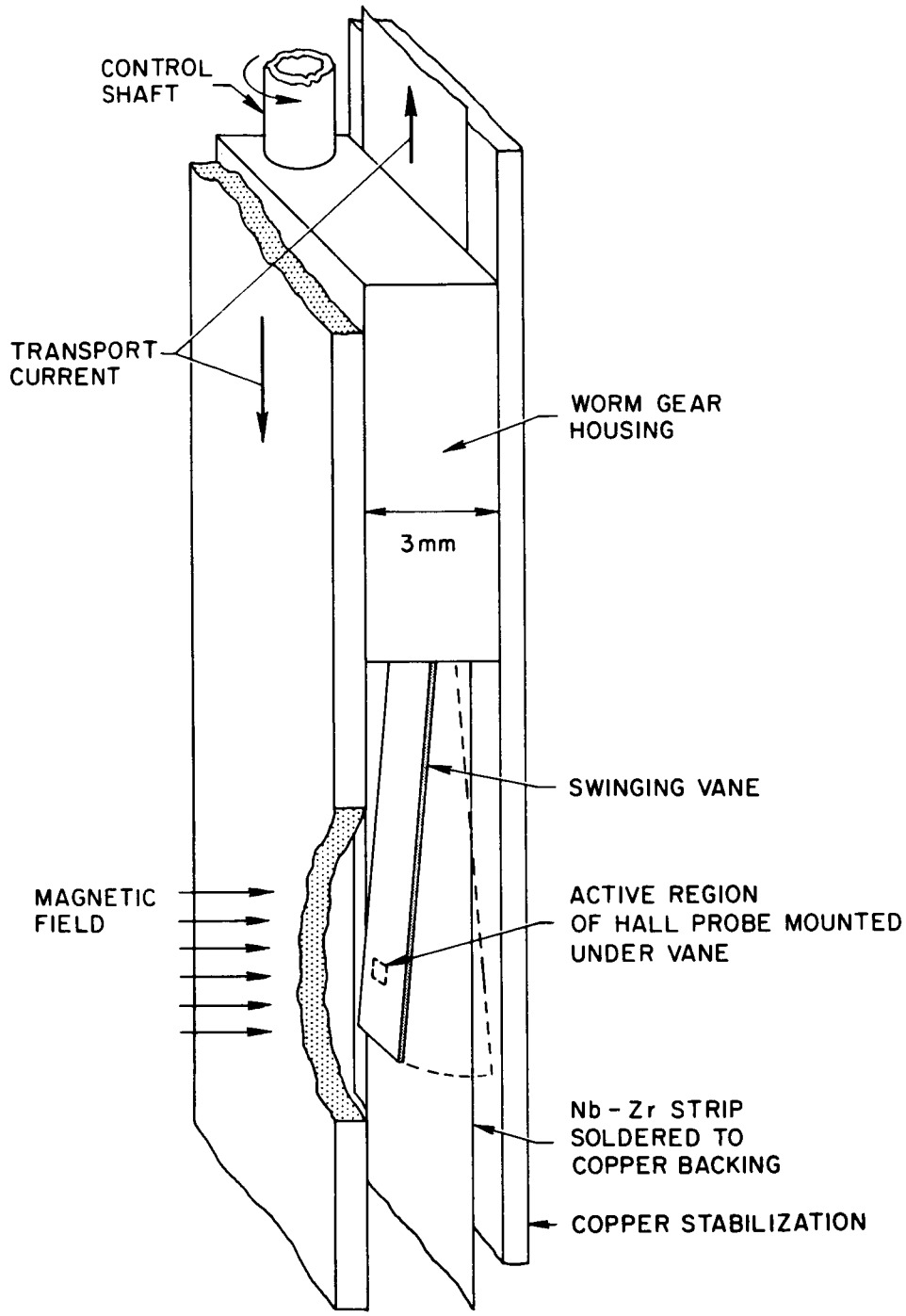

Fig. 1 Details of the Hall Detector Magnetic Field Scanning Apparatus Mounted in Place on the Sample

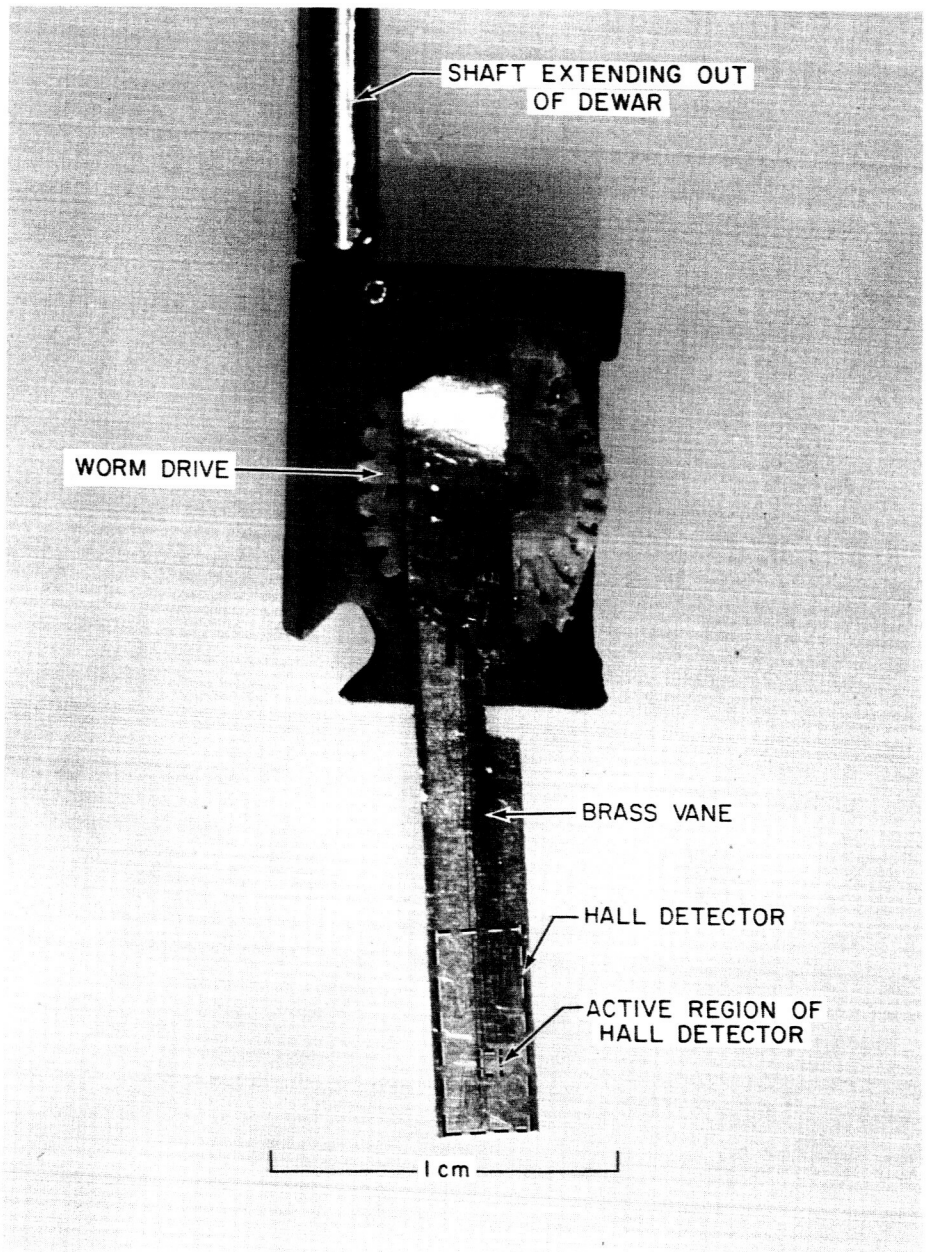

Fig. 2 Photograph of the Hall Detector Scanning Mechanism Showing Details of the Worm Drive Assembly

1. 16 scans at zero external field on a stabilized, virgin sample with no external heating. Transport current was varied in steps ranging from zero up to 450 A, from 450 A to -450 A, then a final scan at zero current. Emphasis here was on obtaining data on relatively low currents.

2. 28 scans at zero external field on a stabilized virgin sample with no external heating. Transport current ranged from zero to 3600 A, from 3600 A to -3600 A, from -3600 A to zero.

3. 30 scans with an external field of 0.076 Wb/m^2 perpendicular to the rolling plane. Transport current ranged from zero to 1800 A, from 1800 A to -1800 A, from -1800 A to zero and a final scan after heating to remove trapped currents.

4. 25 scans with zero transport current and a varying magnetic field perpendicular to the rolling plane. The field ranged from zero up to 0.535 Wb/m^2, from 0.535 Wb/m^2 to -0.535 Wb/m^2 and from -0.535 Wb/m^2 to zero.

After delaminating the sample in the test section to render it unstable, a second series of scans was performed as follows:

1. 27 scans with zero external field. The transport current ranged from zero up to 1800 A, from 1800 A to -1800 A and -1800 A to zero.

2. 17 scans with an external field of 0.076 Wb/m^2 perpendicular to the rolling plane. Transport current ranged from zero to 1800 A, from 1800 A to -1800 A and from -1800 A to zero.

With the sample stabilized (the first series of scans), the observed field distribution changed smoothly and there was no evidence of flux jumping or erratic behavior. The second set, taken after delaminating, however, showed a considerable tendency toward flux jumping. Observed field distributions would change suddenly and unpredictably as the field and transport current were changed.

Data Analysis

The method chosen here for analyzing the field profiles is essentially one of matrix inversion. The strip is divided up into a finite number of sections, each with its own finite current and the field at each point along the path of the scanner is written in terms of a summation of these discrete currents.

The equations are linear since the Hall device is sensitive only to the normal component of the field and consequently can be solved on the computer by matrix inversion.

With reference to Fig. 3, the normal component of the field at any observation point is given by

$$B_{my} = \sum_{-N}^{N} \frac{\mu_o i_n (x_m - x_n)}{2\pi\left[(s_m - x_n)^2 + (y_m - y_n)^2\right]}$$

where m designates a position at which the field is measured and n designates the position of the current element. The computer has been coded for a 42 by 42 matrix and consequently the field data from the experimental profiles is entered in terms of 42 field values. The actual values of x_m, x_n, and y_n are entered in tabular form so that complete freedom is maintained with respect to the resolution of observation points.

Using a known field distribution calculated from a strip carrying a uniformly distributed current, this program has produced satisfactory results. However in applying it to actual data certain problems arise which are not as yet resolved. These are concerned with the accuracy to which the edges of the strip can be located in relation to the field profile data and errors in this positioning estimate can substantially effect the calculated current profile. In the process of ironing out these problems some results have become available, an example of which is shown in Fig. 4. This illustrates the field and current profiles for a 7.6 mm by .051 mm strip in zero external field carrying a transport current of 148 A. While exhibiting certain anomolous features due to positioning inaccuracies (e. g. the current is shown as negative beyond the edge of the strip) it nevertheless illustrates the general character of the current distribution, and establishes with a considerable degree of confidence that the current does in fact tend to travel on the edges of strips. Preliminary examination of the input data not yet reduced also reveals that there is a considerable amount of hysteresis in the field profiles as the external field and transport current are varied, so that substantial losses could be expected in any AC application, particularly where perpendicular fields are encountered. Profiles taken on the sample after delamination reveal sudden unpredictable re-distribution of current. This behavior tends to strengthen the view that the truncation effects mentioned elsewhere in this report are caused by flux jump activity and can be eliminated by good electrical contact to the substrate and good thermal contact to the helium bath.

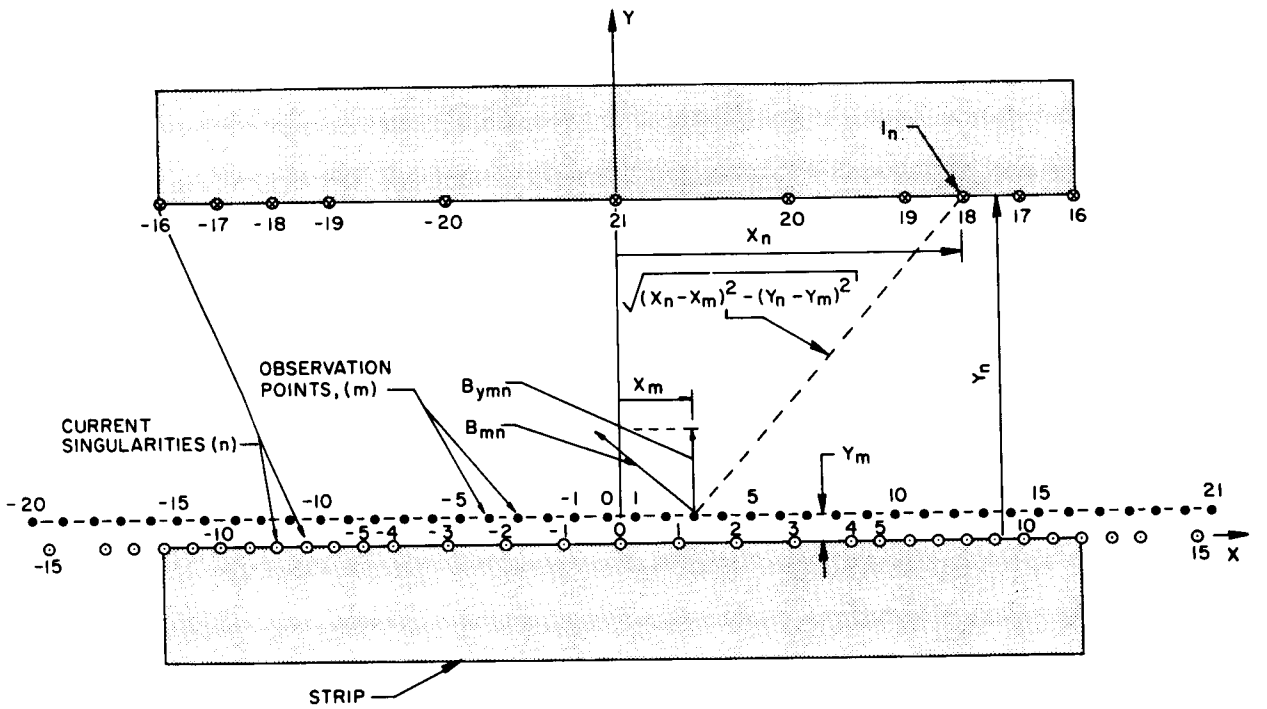

Fig. 3 Details of the layout of observation points and current singularity positions for calculating the current distribution from the field profiles.

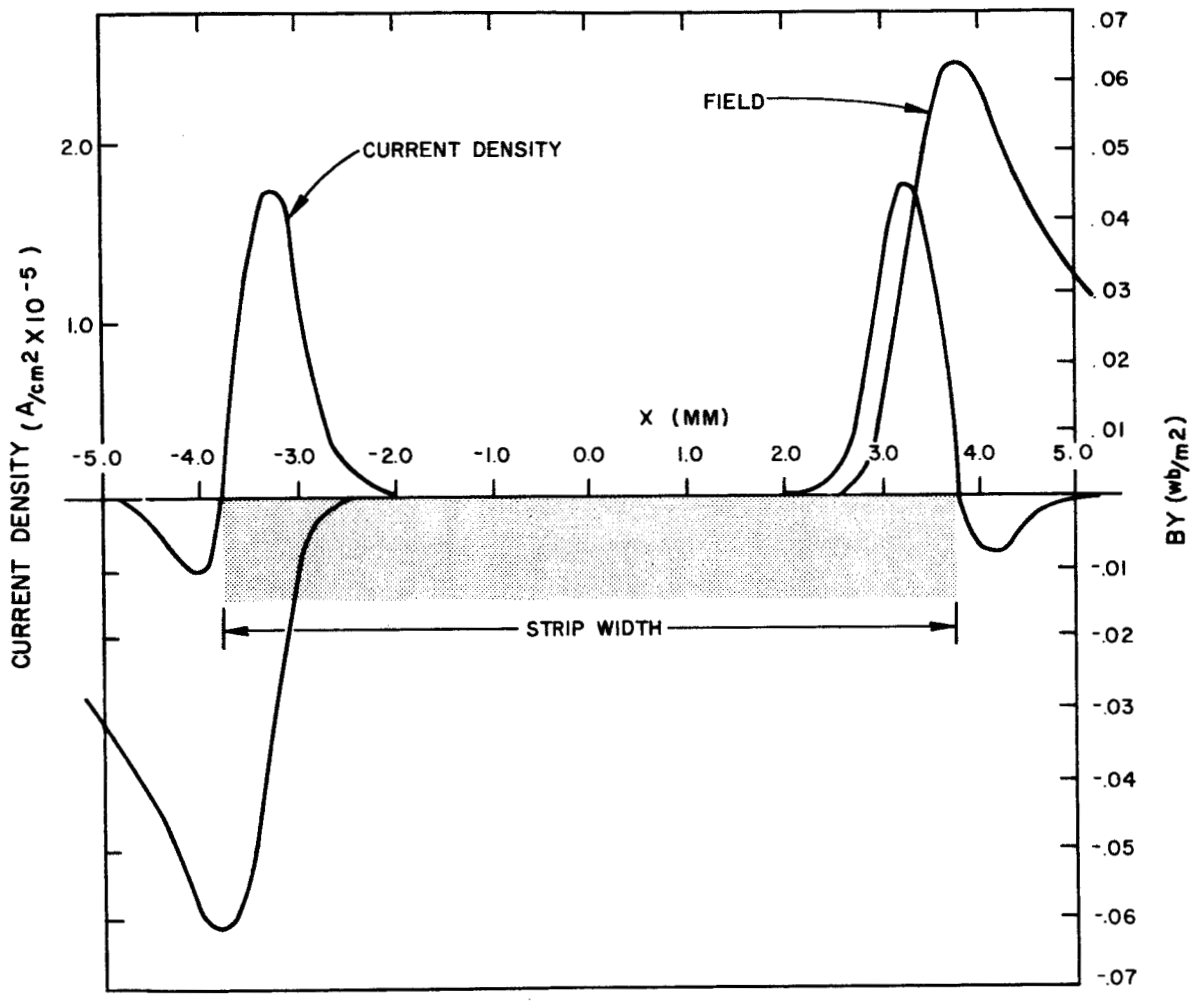

Fig. 4 Typical Current Distribution and its Field Profile

A5417

III. OPERATION OF A FACE COOLED NB-ZR STRIP MAGNET

The necessity for efficient heat transfer from the conductors to the helium bath in stabilized superconducting magnets has been amply demonstrated in earlier work under this contract[3, 4] and elsewhere[5]. This heat transfer must be provided without seriously detracting from the support structure or the electrical insulation and since these are basically conflicting requirements a compromise must be arrived at among them. This compromise is fundamentally a tradeoff between the surface area directly exposed to the bath and the channel width for boil-off vapor to escape. At one end of the spectrum the exposed area is large at the expense of very small passages out of the winding (face cooling) while at the other end a small fraction of the surface is exposed and large passages are provided (edge cooling).

So far under this contract only edge cooling has been investigated. Consequently a face cooled unit was constructed in order to explore the other end of the spectrum. It is shown in Fig. 5 and its specifications are listed in Table I.

TABLE I

I. D.	2.54 cm
O. D.	10.0 cm
Length	12.0 cm
Total turns	168
Inductance	1.53 mH
Field-Current ratio	$1.55\ 10^{-3}$ Wb/m^2 A
Maximum central field	3.0 Wb/m^2
Maximum current	1940 A
Overall current density	$7.27\ 10^{3}$ A/cm^2
Current density in superconductor	$3.00\ 10^{5}$ A/cm^2
Mass of superconductor	.089 kg
Mass of copper	2.82 kg
Dimensions of superconductor	.051 mm by 12.7 mm

It consisted of eight modules wound on a single mandrel all connected in series, and its construction was as shown in Fig. 6 where one quadrant is shown in section. A special winding technique was developed to wind all eight modules from a single length of strip with no jounts. The individual

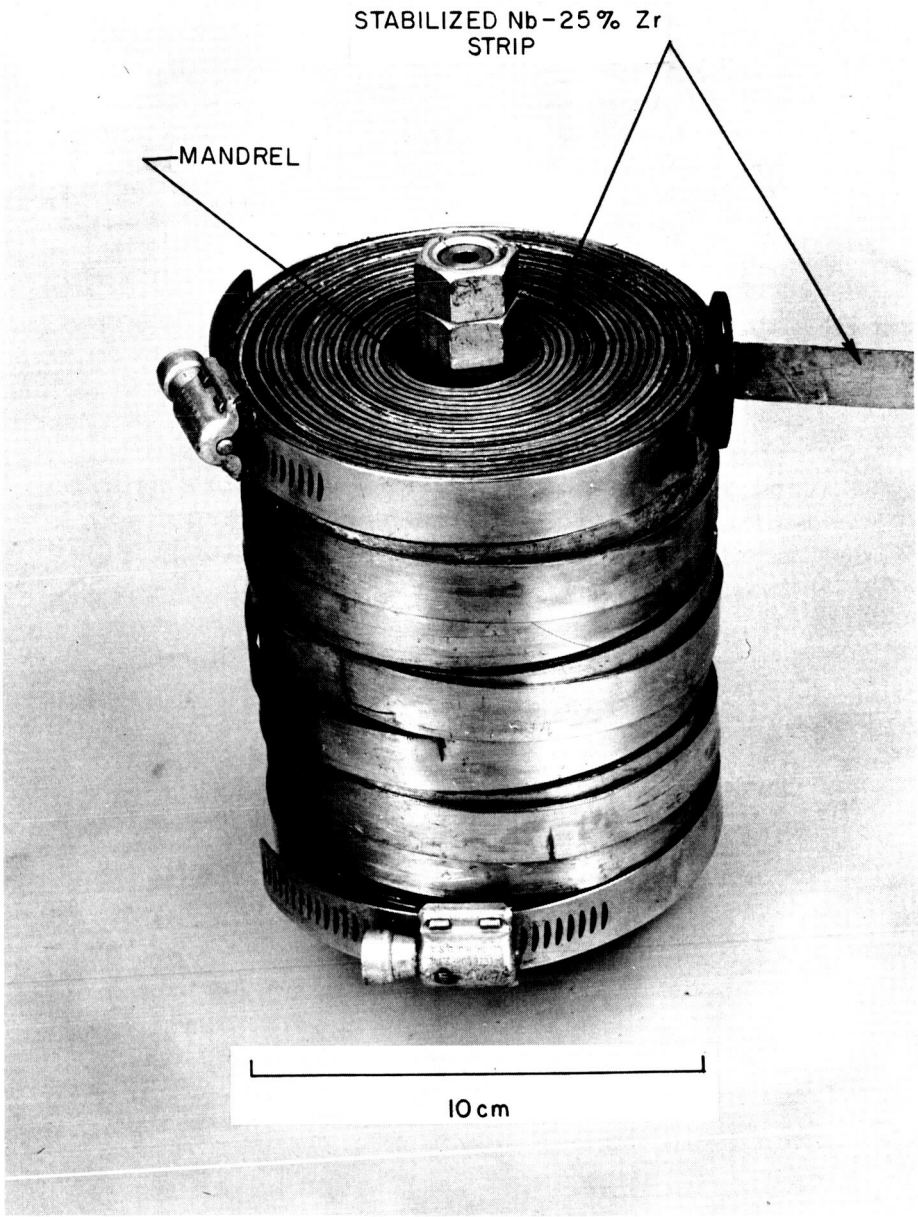

Fig. 5 Face Cooled, Stabilized Nb-Zr Strip Magnet. This unit operated on the H-I curve and produced a central field at 3 Wb/m^2 with a current of 1940 A.

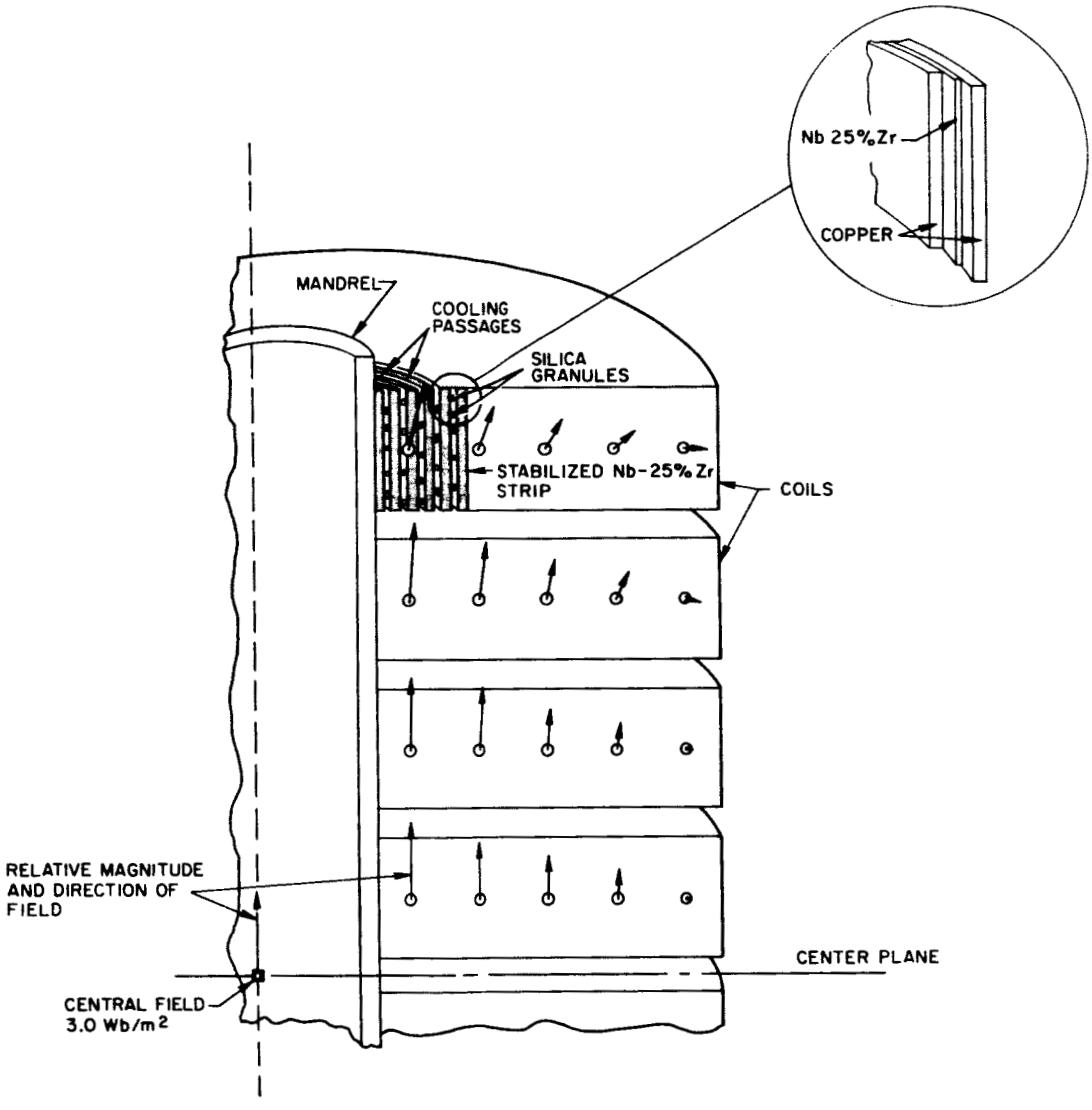

Fig. 6 Field Profile and Structural Details of the Face Cooled Strip Magnet. The vectors indicate the relative magnitude and direction of the field in winding.

turns of each module were spaced from one another by granules of silica held in place by the winding tension. This provided a method of insulating the turns from each other while providing a narrow channel for vapor to escape. The strip conductor itself consisted of optimally annealed Nb-25% Zr strip 0.051 mm thick by 12.7 mm wide soldered between two copper strips 0.38 mm thick by 12.7 mm wide. The separation provided by the silica granules was approximately 1.7 mm.

Each module was provided with 8 voltage taps and these were distributed to provide the greatest resolution near the center where the magnet first shows a voltage when the critical current is exceeded. Working out from the center, taps were provided (all at the same azimuth) on the following turns: 1, 2, 3, 4, 5, 10, 15, 21. The unit was tested with its center axis vertical in the field of another magnet capable of producing 2 Wb/m^2 and a 33 channel magnetic tape recorder was used to monitor the tap voltages, the magnet current and the central field.

The test consisted of running the magnet in bias fields ranging from zero to 2 Wb/m^2 and monitoring the normal voltages appearing in the magnet as the critical current was exceeded. In this way, an H-I characteristic for the magnet was determined as shown in Fig. 7 where it is shown compared with the H-I characteristic of the strip from which it was wound. The experimental points for the magnet are slightly higher than those for the short sample because the magnet voltage was measured with a less sensitive meter.

The short sample H-I characteristic is for the parallel field direction showing that for a magnet of this shape the anisotropy poses no serious problem. As seen from Fig. 6, the regions of the winding in which its field direction differs greatly from parallel are low field regions and consequently do not limit the currents. To this extent the coil can be considered automatically graded.

In all the tests made, the magnet operated stably in the sense that the normal voltage was single valued for a finite range of currents above the critical current where a voltage first appeared. If this finite range was exceeded, an irreversible voltage would develop which disappeared at a recovery current somewhat less than critical. The greater the critical current, the less the stable range above that current and the lower the recovery current once that range was exceeded. This effect is illustrated in Fig. 8 where three actual recovery curves are shown as recorded by an X-Y recorder set up to indicate the total coil voltage. As long as the magnet current is kept within the reversible region, the voltage disappears on returning to the critical value.

In order to investigate the origin of the unstable or irreversible part of the V-I curve the voltages from the coil taps inside the winding were recorded simultaneously. The voltages between taps 1, 2, 3 and 4 on each of the eight modules were all recorded. By comparing the currents at which voltage first appeared between the various taps, a map of the normal region

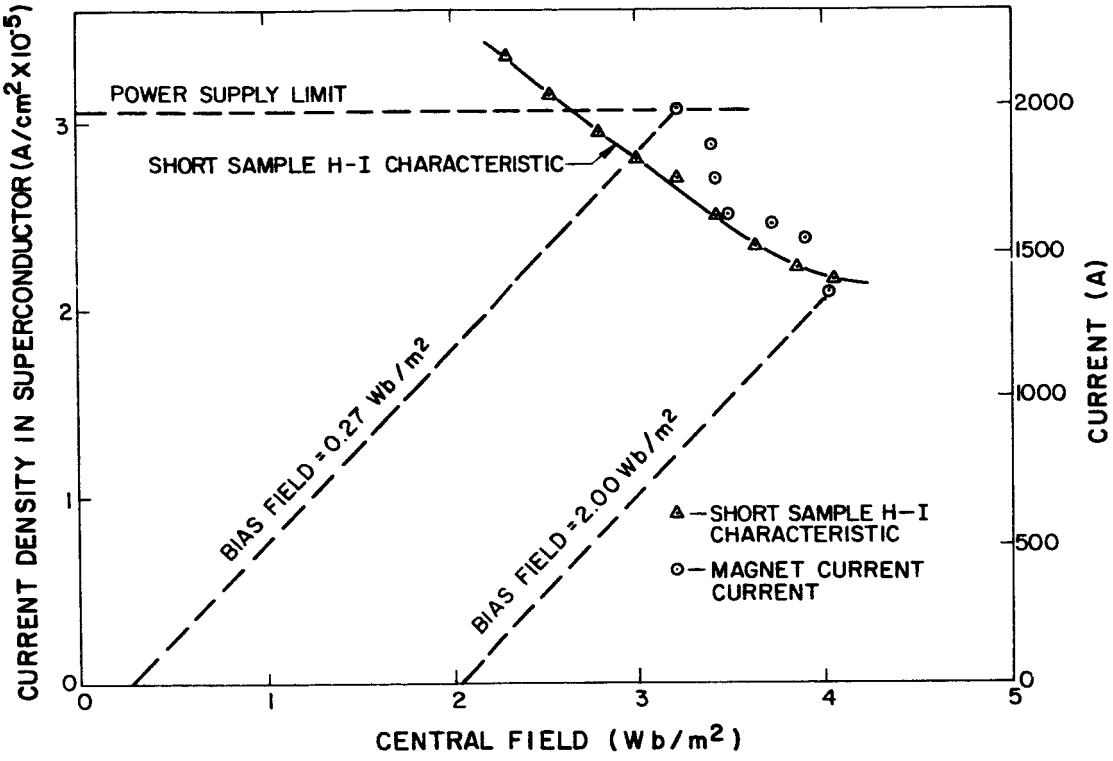

Fig. 7 Comparison of Face Cooled Strip Magnet Performance with H-I Curve. The data was obtained by operating the magnet in the bias field of another magnet.

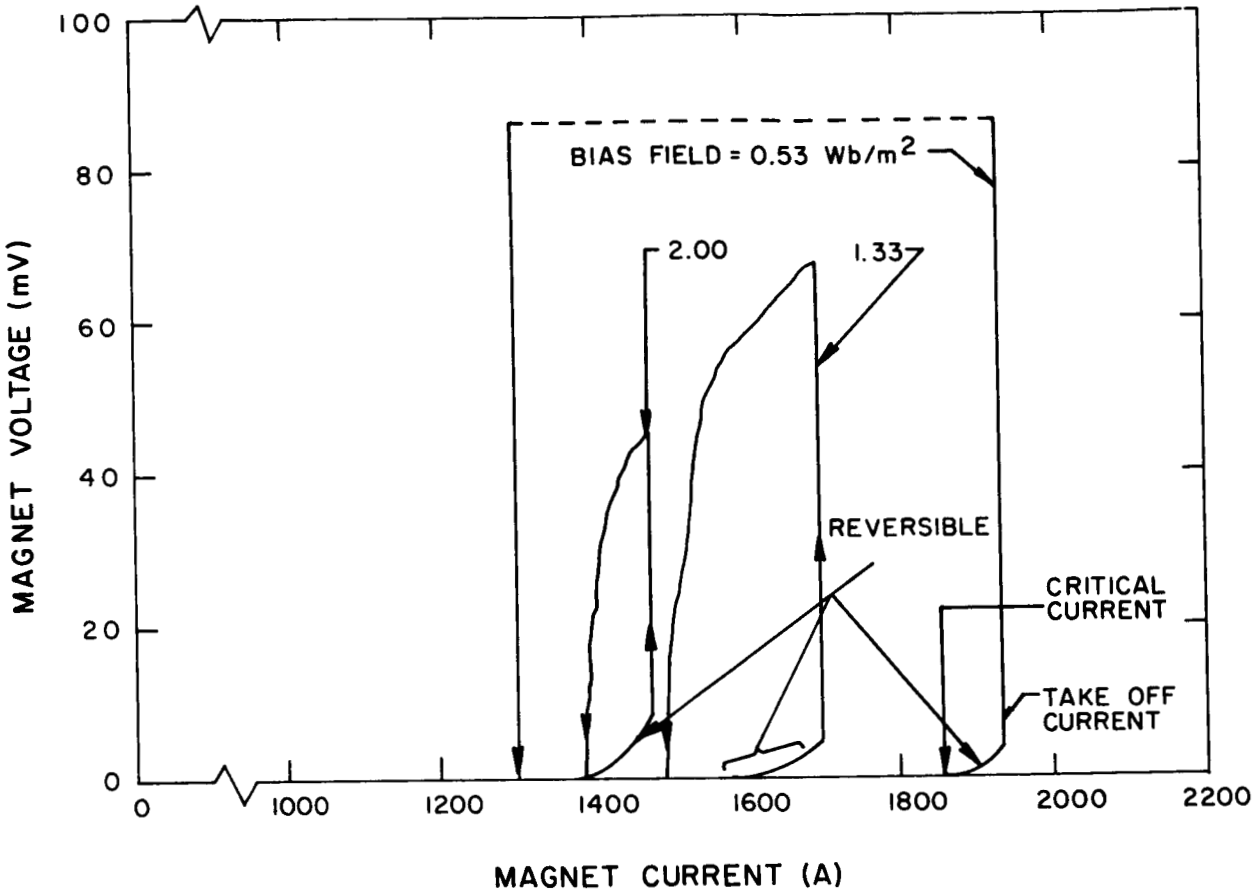

Fig. 8 Typical Voltage-Current Characteristic for the Face Cooled Strip Magnet. The unit operates reversibly on the curved portion between the critical current and take-off current but exhibits hysteresis with currents above the take-off value.

at any given current could be constructed. This was done both for the critical currents where voltage first appears and for the "take-off" current where the voltage becomes irreversible.

The results are shown in Fig. 9 which is a schematic map of the normal region which occurred with bias field of 1.33 Wb/m^2. Each square there represents a single turn of a single module of which the first four turns are shown. The cross hatching indicates a stable or reversible voltage while the shading represents unstable or irreversible voltage. The numbers in each square indicate the current at which the voltage first appeared in each turn, the lower number indicating the onset of reversible voltage and the upper number the onset of irreversible voltage.

The reversible normal region appeared to start at 1580 A in the cross-over between modules D and C and progress out radially from there as the current was increased. The irreversible voltage first appeared in the cross-over between modules E and F and spread outward and upward as the current was increased. The important aspect of this map is the fact that whereas the stable region spread out radially from approximately the center (as would be expected in view of the field distribution shown in Fig. 6) the unstable normal region affects only the upper modules which are bathed in the boil-off bubbles rising up from the lower modules. This shows that the stability is critically dependent upon the quality of the coolant as well as the amount of surface exposed.

The surface heat transfer rate can be calculated by assuming that all of the Joule heating generated in any given section escapes via the surface area in that section. For the case shown in Fig. 9 the surface heat transfer rate for a current just below the take-off value was calculated to be approximately 0.03 W/cm^2 while just above the take-off value it was 0.5 W/cm^2. Assuming a copper resistivity of $2\ 10^{-8}\ \Omega/cm$ at 4.2°K the current in the copper just below take-off is 815 A indicating that the current is being shared by the superconductor and copper. In the unstable region just above the take-off point the voltage level indicates that all of the current is in the copper and that its temperature is approximately 20°K as calculated from resistivity temperature curves for copper. This is a so called "burn-out condition" in which film boiling has set in and is limiting the heat transfer.

In general it appears from this experiment that the advantages to be gained by the increased surface area exposed to the helium is offset to a considerable degree by the rather limited passage width. The narrow passages inherent in a face cooled design tend to be much more susceptible to choking by the vapor bubbles than the broad passages in the edge cooled designs. This limitation however can probably be overcome by operating below the lambda point, where vapor cannot exist, or above the critical point where there is no difference between the liquid and vapor. Face cooled designs, therefore, do not appear to be ruled out and further investigation is indicated.

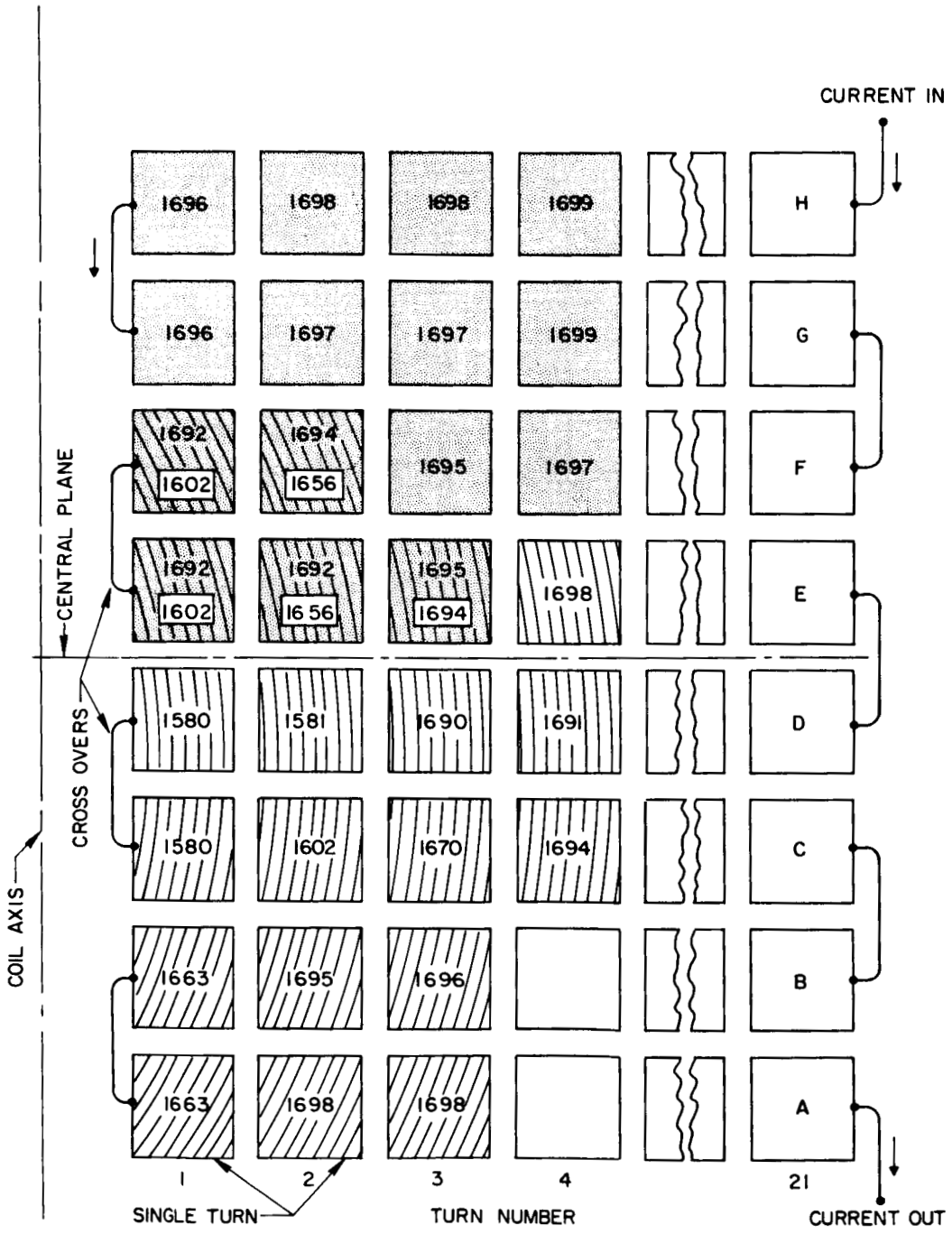

Fig. 9 Schematic Stability Map of the Face Cooled Strip Magnet. Each square represents a single turn of the winding, the cross hatching indicates reversible normal regions, the shading indicates irreversible normal regions and the upper and lower numbers indicate respectively the currents (in amperes) at which these irreversible and reversible states first appear.

IV. OPERATION OF SUPERCONDUCTORS AT TEMPERATURES BELOW THE LAMBDA POINT

In the work outlined above with the face cooled magnet, it was concluded that the irreversible mode of operation was due mainly to the presence of helium boil-off vapor generated from other parts of the magnet. One obvious remedy for this situation is to operate the magnet at temperatures below the lambda point, since no vapor can exist then to disrupt the heat transfer. In order to test this possibility, a low temperature facility was constructed and a small magnet was tested.

The low temperature facility consisted of a 6" I. D. glass dewar assembly arranged so that its internal pressure could be reduced by means of a vacuum pump. The temperature was estimated by monitoring the pressure with an aneroid vacuum gauge and the presence of superfliud helium could be readily confirmed by visual observation as well as by pressure measurements.

The magnet consisted of a single pancake type coil 2.54 cm I. D. by 10 cm O. D. wound from a stabilized Nb-25% Zr conductor consisting of a 0.25 mm diameter wire imbedded in a rectangular copper conductor 1.0 mm x 3.7 mm. It was equipped with a heater near the inner radius, and removable phenolic side plates were provided so that it could be operated in one of two heat transfer regimes. With the side plates removed, the edges were directly exposed to the bath and when in place they fitted snugly, but no attempt was made to seal them.

Two tests were conducted, one with the side plates in place and one with them removed. Each test consisted of energizing the magnet with various heat inputs applied and observing its voltage-current characteristics. This was done at three different temperatures, 4.2°K, 2.2°K (just above the lambda point) and at 2.0°K (below the lambda point), so that the effects of the superfluid could be separated from those due to the lowering of the temperature. The data at 2.2°K show the effect of lowering the temperature while those at 2.0° show in addition, the effect of the superfluid.

A typical voltage-current characteristic for the unit is shown in Fig. 10. As seen there the magnet is partially stable in the sense that although the transition is sudden, it recovers without returning the current to zero. Current sharing is evident as witnessed by the fact that if the normal part of the curve in Fig. 10 is extrapolated back to zero voltage it intersects the current axis at a finite current (i.e., 103 A). This implies that some of the current does in fact remain in the superconductor although the transition is not a smooth one. Evidently a portion of the total current suddenly transfers out of a more or less fixed length of conductor, leaving a constant amount behind in the superconductor. The excess is then manifested by a linearly increasing terminal voltage as the total current is increased.

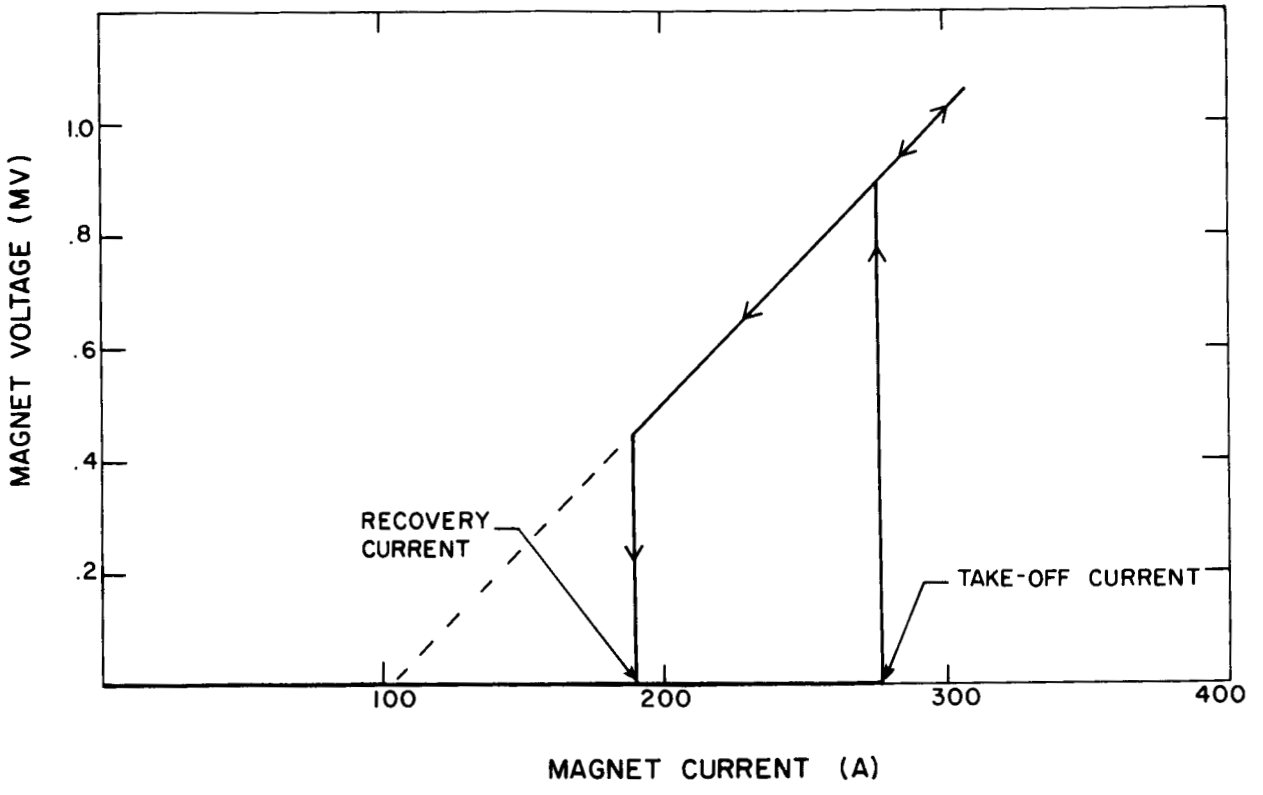

Fig. 10 Typical Current-Voltage Characteristic for the Low Temperature Magnet. Extrapolation to zero voltage indicates current sharing, although the transitions are not smooth.

A5413

Following this model results in a copper conductivity of 4.40×10^{-8} cm and a heat transfer rate ranging from .035 W/cm^2 at the recovery point to .102 W/cm^2 at the take-off point. Judging from the results of the face cooled magnet, these numbers are quite plausible, lending credence to the assumed model.

With this model in mind, the overall characteristics of the magnet can be discussed. These are shown in Figs. 11, 12, and 13 where the recovery and take-off currents are plotted as a function of heater power for the three different temperatures and for the two heat transfer environments. They illustrate the characteristic at temperature of 4.2, 2.2, and 2.0°K, respectively and the two heat transfer environments are superimposed in each figure. The most significant fact illustrated by these plots is that the presence of superfluid helium substantially reduces the effects of the side plates. When they are removed, the unit behaves approximately the same at all temperatures, but with the side plates in place the heater power is depressed significantly for the two temperatures above the lambda point, while below the lambda point it behaves roughly the same with and without the side plates.

In all cases the unit performed essentially on the H-I curve as would be expected for a magnet this small, and at the lower temperatures slightly higher currents are obtained. This is due to the slight raising of the H-I curve in going from 4.2° to 2.0°. No improvement in stability is noted however on going below the lambda point and this is probably due to the partially stable behavior of the conductor with which the magnet was wound.

Although there is definite evidence of current sharing, the transition was not smooth so that at the higher currents the transition resulted in a Joule heat generation in excess of the surface heat transfer consistent with stable operation. The value of 0.1 W/cm^2 implied by the case illustrated in Fig. 10 is already quite high, judging by the face cooled coil experiment and consequently, it probably takes only a slight increase to cause a complete "burnout" condition. The conductor used in this experiment was slit by a sawing technique from nine wire SG700 Supergenic Strip and it is quite possible that the rigors of slitting and winding disrupted the bond sufficiently to cause the partially stable performance.

The conclusions that can be drawn from the experiment are:

1. That the presence of helium II definitely improves the heat transfer environment.

2. That its ability to extract heat is limited (probably by some maximum temperature gradient) to the extent that it could not support the heat generation in the partially stable material.

In spite of its limitations, helium II represents considerable promise for magnet construction because it should relieve the rather stringent structural requirements inherent in present designs which must combine good heat transfer with high strength.

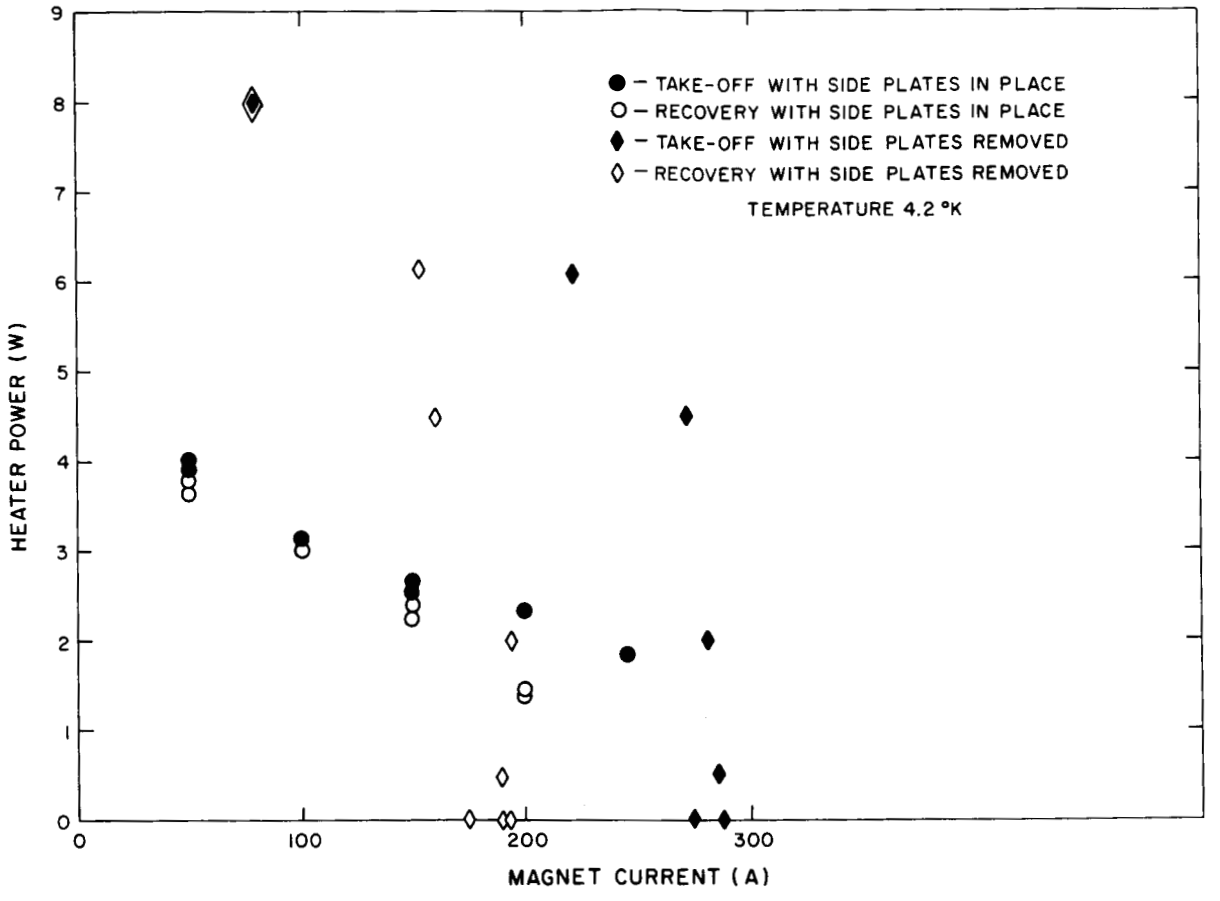

Fig. 11 Stability Map for the Low Temperature Magnet Operating at 4.2°K, with and without the Side Plates. With the side plates removed, significantly less heater power is needed to produce a normal voltage.

A5412

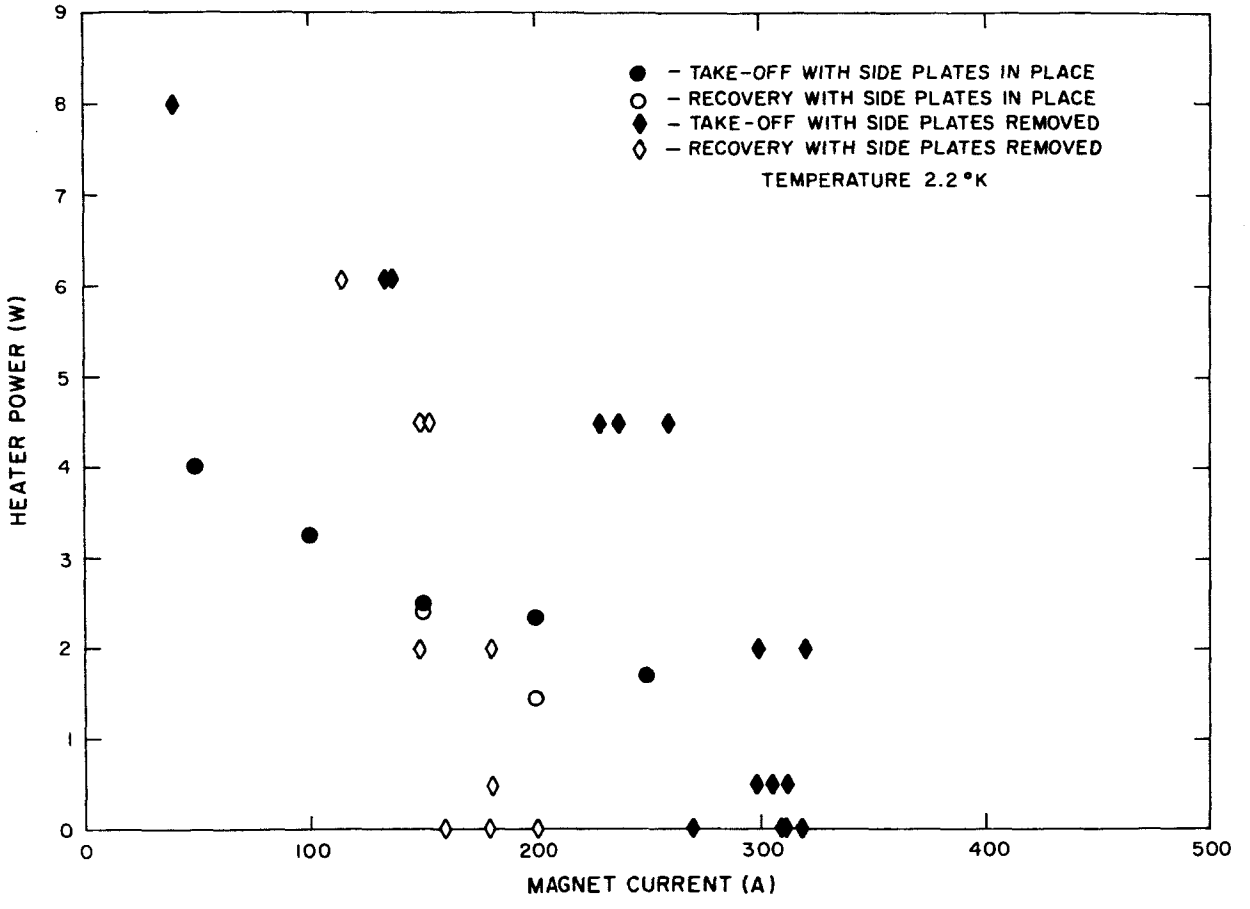

Fig. 12 Stability Map for the Low Temperature Magnet Operating at 2.2°K with and without the Side Plates. With the side plates removed, significantly less heater power is needed to produce a normal voltage.

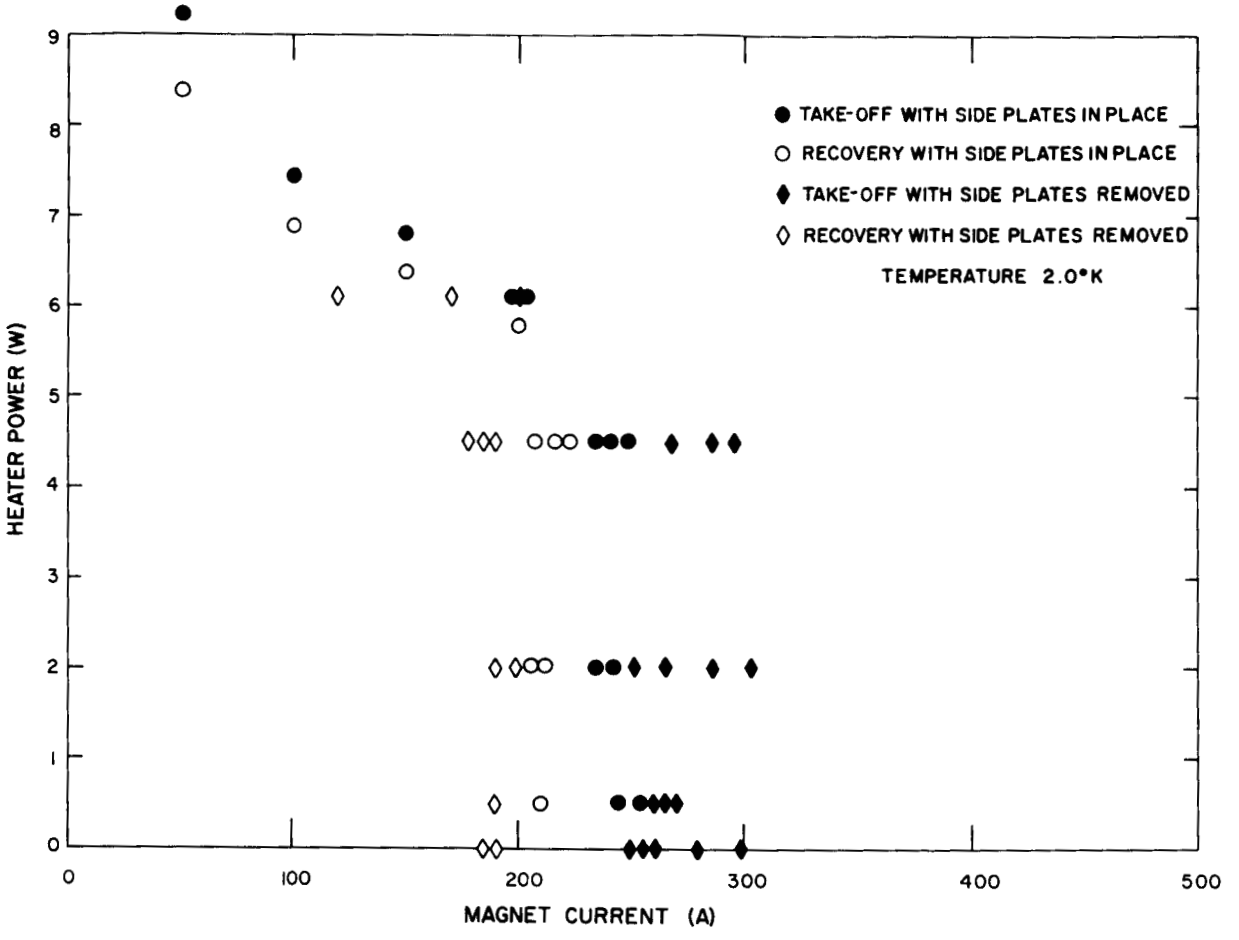

Fig. 13 Stability Map for the Low Temperature Magnet Operating at 2.0°K with and without the Side Plates. The side plates make little difference in the heater power necessary to produce a normal voltage.

V. BOILING HEAT TRANSFER TO LIQUID HELIUM IN VERTICAL PASSAGES

The successful design and construction of stabilized superconducting magnets is dependent on the heat transfer between the conductor and the liquid helium environment. In order to operate in a stable manner, the conductor must be able to reject to the liquid helium the Joule losses generated by the design current while staying below the critical temperature of the superconductor. Since critical temperatures are well below 20°K, and the saturation temperature of liquid helium at atmospheric pressure is 4.2°K, only heat transfer processes which take place at small temperature differences are important.

Only nucleate boiling, and natural and forced convection take place in liquid helium at temperature differences in the range of 5 - 10°K.[6] Film boiling takes place only at considerably higher temperature differences. The usual method of operation for superconducting magnets consists of complete immersion in liquid helium.[7] There is no forced circulation, and most superconducting magnets experience only natural circulation as a result of density change due to temperature changes or boiling in the liquid helium. The heat transfer to liquid helium attainable with natural convection is limited to values well below 0.1 watt/cm^2.[6]

The region of real interest for stabilized conductors simply immersed in liquid helium is the nucleate boiling region. In general, this region covers the range between the onset of nucleate boiling and burnout. Burnout is the point where the highest nucleate heat flux is achieved and further increase in heat flux forces a transition to the film boiling region at considerably higher temperature differences.[8] Unfortunately most stabilized conductors cannot be designed for heat fluxes near the burnout point. The burnout heat flux can be obtained from a surface in an unconfined helium environment where liquid helium can replace the vapor generated at the surface. In a narrow passage, the rate at which liquid is supplied to the boiling surface is determined by the hydrodynamics of the flow in that passage. The difference between the hydrostatic heads inside and outside the passage provides the driving force for the flow rate through the passage. If the liquid helium boils faster than it can be supplied, the passage becomes vapor bound and the heat flux can be accomodated only at higher temperature differences.

It is therefore important to obtain a correlation between the passage dimensions, the maximum nucleate boiling flux, and the mass fraction of vapor leaving the passage. In order to obtain early quantitative results, some experimental runs were made on a vertical passage submerged in liquid helium.

Test Equipment

The significant quantities to be measured in the test runs are wall temperature, saturation temperature, heat flux, exit quality and pressure drop. The test section is designed to allow measurement of these quantities. The test section shown in Fig. 14 consists of a 30 cm circular channel with wall heaters. There are two 2.5 cm long heaters and one 25 cm long main heater. The channel is made of OFHC copper which has a high thermal conductivity and provides even surface temperatures. The channel diameter is 2.00 cm. The heater element consists of nichrome wire which provides good thermal contact with the copper. Radial heat conduction to the outside is limited by two concentric sections of nylon directly over the copper heater sections. The entire assumbly is held in place by two stainless steel end flanges. The bottom flange is faired to provide a smooth transition region for the inlet flow. The top flange has a raised lip which forms an annular groove to collect carryover liquid. The channel is equipped with a removable center plug, which forms an annular passage. The center section which has a diameter of 1.27 cm, is centered in the channel by means of standoffs fastened to the center section. The lower end of the center section ends in a smooth faired cone which provides a smooth inlet transition region. At the top of the center section, a deflector shaped like an inverted funnel directs the overflow liquid helium into the collect annulus. The entire center section is suspended through the deflector from a plate located some 8 cm above the test section. A glass sleeve confines the carryover liquid helium to the collect annulus. Carbon resistance thermometers are embedded in the copper channel wall. The main heater has four carbon resistance thermometers, the two small heaters have a single thermometer each, one a carbon, the other a germanium resistance thermometer. The germanium thermometer is used for calibration and checking purposes. The instrument and heater leads are brought out through the nylon insulating sleeve. The heater leads are #22 copper starting right at the nichrome heater to minimize heat generation in the leads.

The entire test section is suspended from the top flange by means of four stainless steel threaded rods, as shown in Fig. 15. A graduated cylinder is positioned along side the test section to collect carryover liquid helium. A small heater in the bottom of the graduated cylinder is used to boil off collected liquid helium, so that the next run can be started with an empty cylinder. The entire assembly is lowered into a 15 cm diameter glass helium dewar as shown in Fig. 15. Styrofoam is used as a plug to limit heat leak from the top.

Test Results

The test equipment was operated to obtain data on both a short local heater segment and a full channel length heater. In both cases the data was obtained with an X-Y recorder, with the current plotted on the Y-axis and the thermometer voltage on the X-axis. Figure 16 shows a typical data plot from the X-Y recorder. The thermometer voltage decreases from right to left as the heater temperature increases. This run was made with the main (large) heater, and the data is reduced into heat flux and temperature

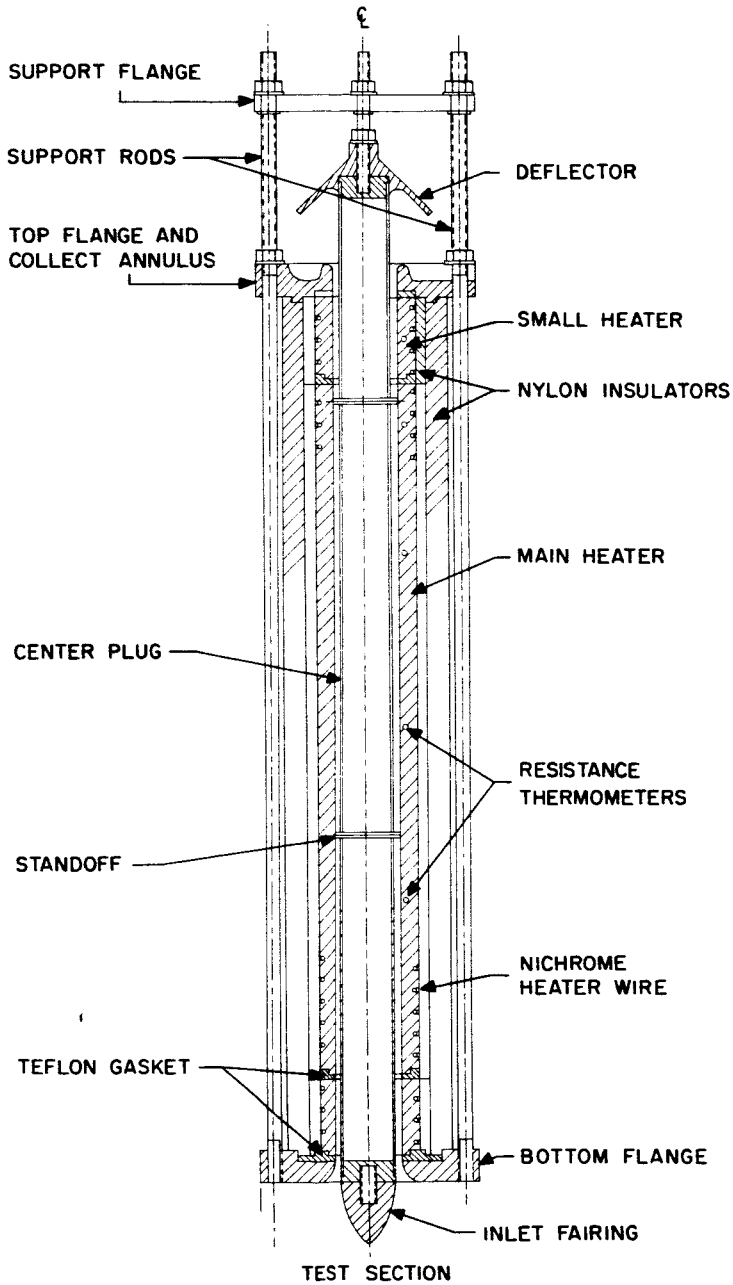

Fig. 14 Test Section Schematic

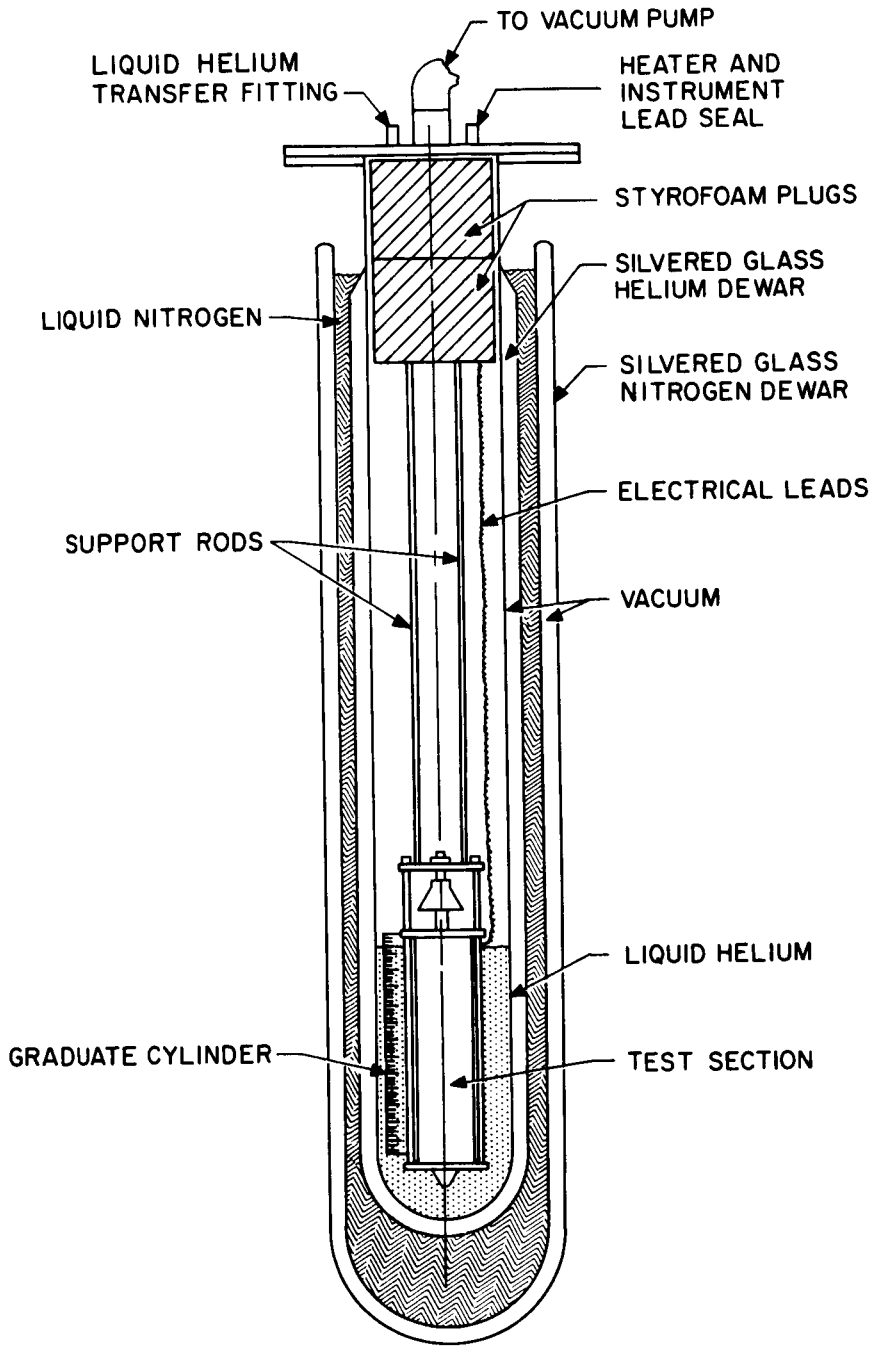

Fig. 15 Test Configuration

A5477

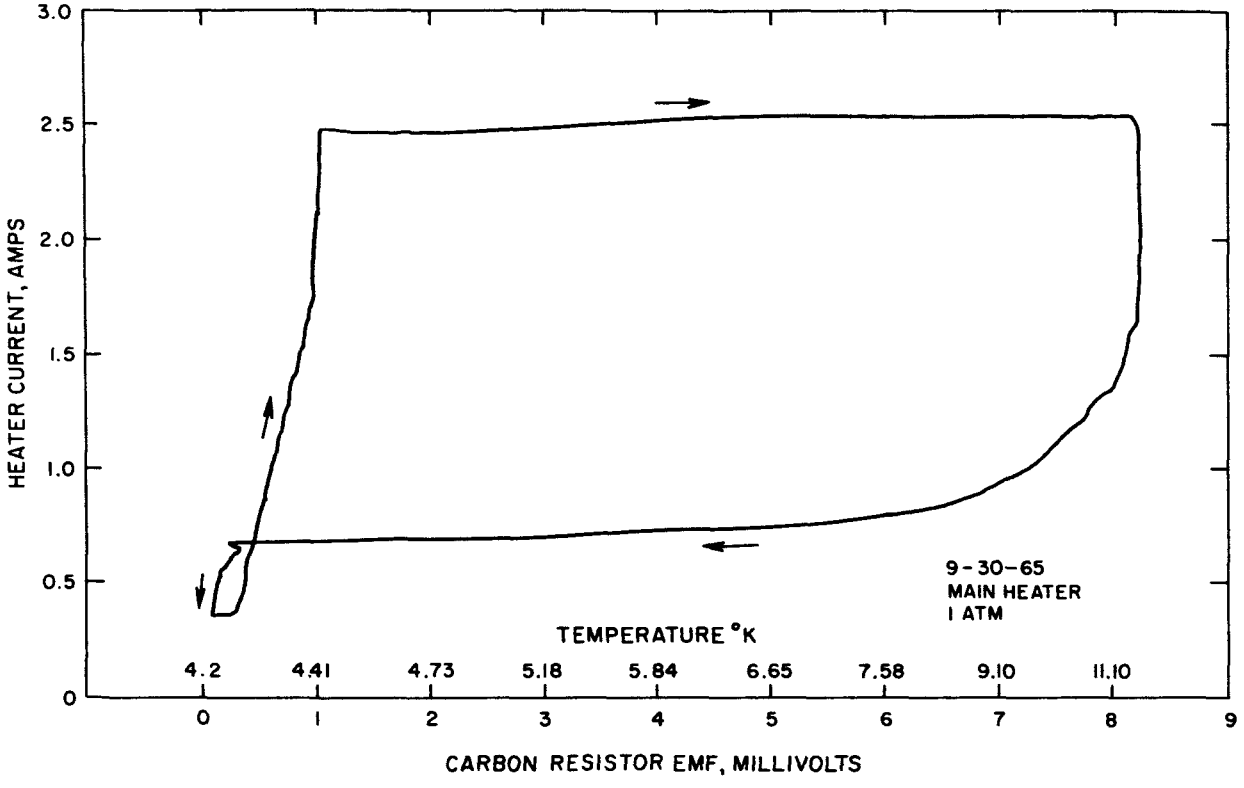

Fig. 16 X-Y Data Recording of Heater Current vs Carbon Thermometer Output Voltage

difference and plotted in Fig. 17. Figure 17 also shows results from one of the small heater runs, which yields higher nucleate boiling heat flux. Test runs were made by gradually increasing the heater power until the transition to film boiling was achieved. At that point the heater current was was reduced until nucleate boiling was again achieved, at which point the run was terminated. The comparison of these two runs clearly shows the effect of vapor choking of the passage. The small heater has a lower vapor generation rate, and results in a lower exit quality. Both curves exhibit a sharp transition at the maximum nucleate boiling heat flux. This suggests that this maximum heat flux value falls short of the burnout heat flux, which is generally characterized by some rounding of the curve prior to transition to film boiling.[8] The maximum heat fluxes are .7 W/cm^2 and .29 W/cm^2 for the small and large heater sections respectively. Both the transition from nucleate to film boiling and the reverse transition take place quickly on the X-Y recorder which indicates that the thermometer response is adequate to record these changes.

The results shown in Fig. 17 present ample evidence that the passage hydrodynamics have a marked effect on the maximum achievable nucleate boiling heat flux. As observed in the operation of the face cooled magnet (and elsewhere as well)[9] the local quality (ratio of vapor mass to total mass of mixture) is very important in determining the maximum nucleate boiling heat flux and the actual heat flux estimated there is in fact approximately the same as that shown here in Fig. 17. A very long passage requires a lower average wall heat flux to reach the critical quality at some given flow rate. This implies that the passage diameter will probably scale with some overall characteristic dimension in stable superconducting magnets. An increase in passage diameter generally decreases the packing factor, unless the conductor in increased proportionately. In short, the attainable heat flux is dependent on the passage dimensions, which in turn determine the magnet configuration.

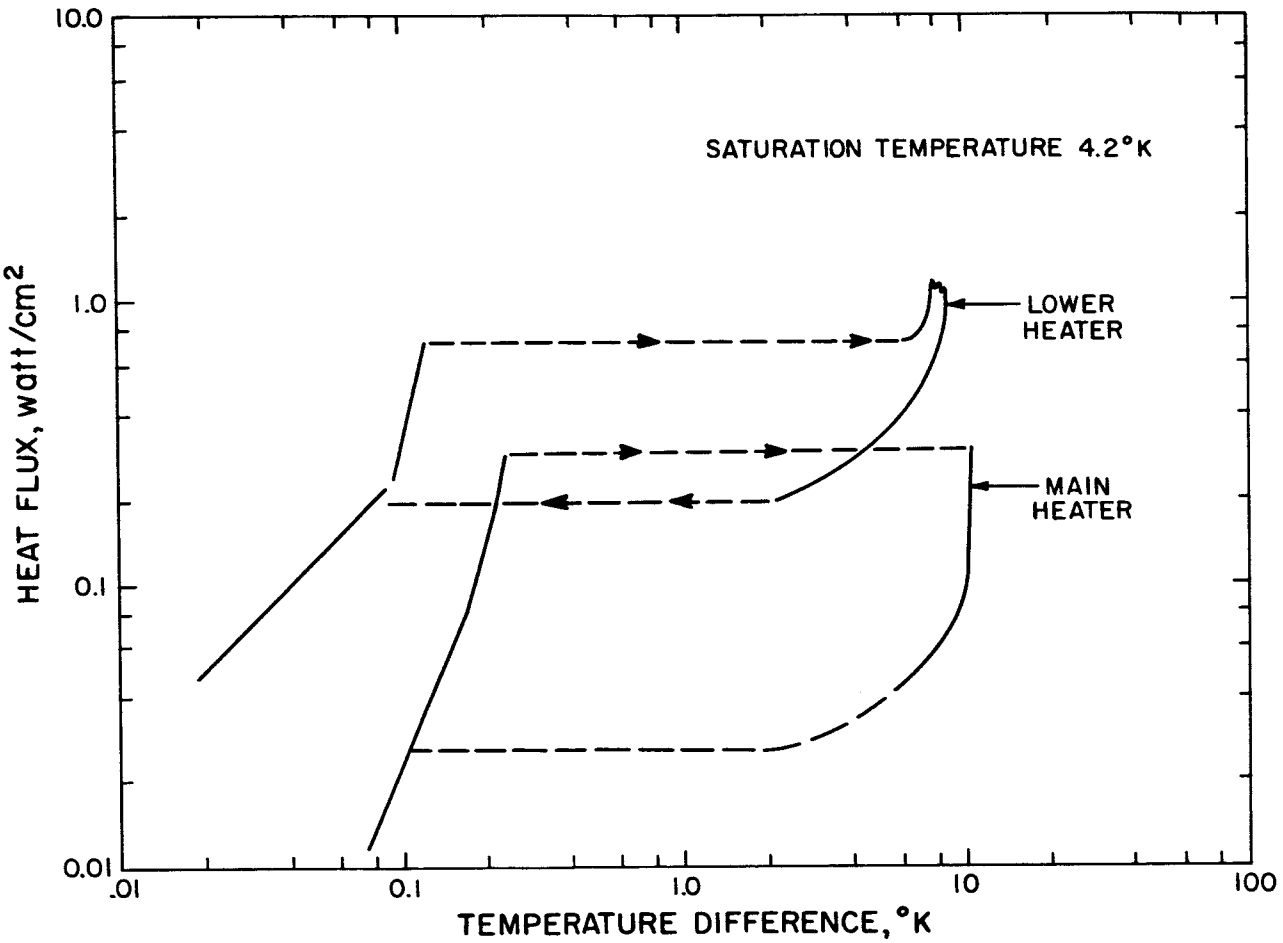

Fig. 17 Heat Flux as a Function of Difference Between Channel Wall Temperature and Liquid Helium Saturation Temperature

VI. A COMPARATIVE ANALYSIS OF SUPERCONDUCTING MAGNET ENERGIZING SYSTEMS

The incentive to develop and use flux pumps to energize superconducting magnets stems mainly from the economics involved in transferring electrical energy from room temperature sources to the magnet at liquid helium temperatures. The fact that good electrical conductors are also good thermal conductors poses a fundamental conflict which tends to place a lower limit on the inductance of the magnet because of the heavy leads then required to energize it. The flux pump tends to alleviate this problem of lead heat leak because it provides an impedance transformation at the low temperature, so that no matter what the inductance, the energizing power can always be fed in at high impedence. High voltage, low current leads with small cross section and negligible heat leak can then be used.

Many authors have proposed the use of flux pumps and several experimental units have been operated[10-16] but very little attention has been paid to the efficiency of these devices. In this section we shall examine in detail the efficiency that can reasonably be expected from flux pumps and compare it with the efficiency for other types of energizing methods.

Although a great variety of flux pump configurations have been proposed[10] they are all fundamentally the same device. In one guise or another they all provide some means for carrying magnetic flux lines through a current carrying region without interrupting that current. As shown in Fig. 18, they can be classed into two types, both of which are predicated on the idea that the flux must remain constant inside any closed zero resistance contour (the contour in this case being the magnet with its terminals shorted by the flux pump). If flux can somehow be introduced into such a contour, it will remain trapped there as long as some part of the contour at least remains closed and at zero resistance. In Fig. 18-A the inductor being charged is shorted by means of a thin sheet of superconductive material and flux "packets" are carried across by passing them through a small normal spot and allowing the spot to move across the strip. The normal spot is small enough to permit the main current to bypass around it. Electrical losses are incurred by virtue of the eddy currents which are induced in the normal metal of the spot by the motion of the flux with respect to the material.

In Fig. 18-B flux is moved in by sequentially opening and closing the switches. Electrical losses occur because of the finite voltage across the persistent switch in its normal state while flux moves in. This voltage is a necessary and sufficient condition for flux to move into the circuit. To obtain electrically lossless operation the switches would have to have infinite resistance in their "open" state and would have to be opened and closed only when the current through them is zero. These conditions can be approached by using mechanical switches but even then losses will still occur in practice

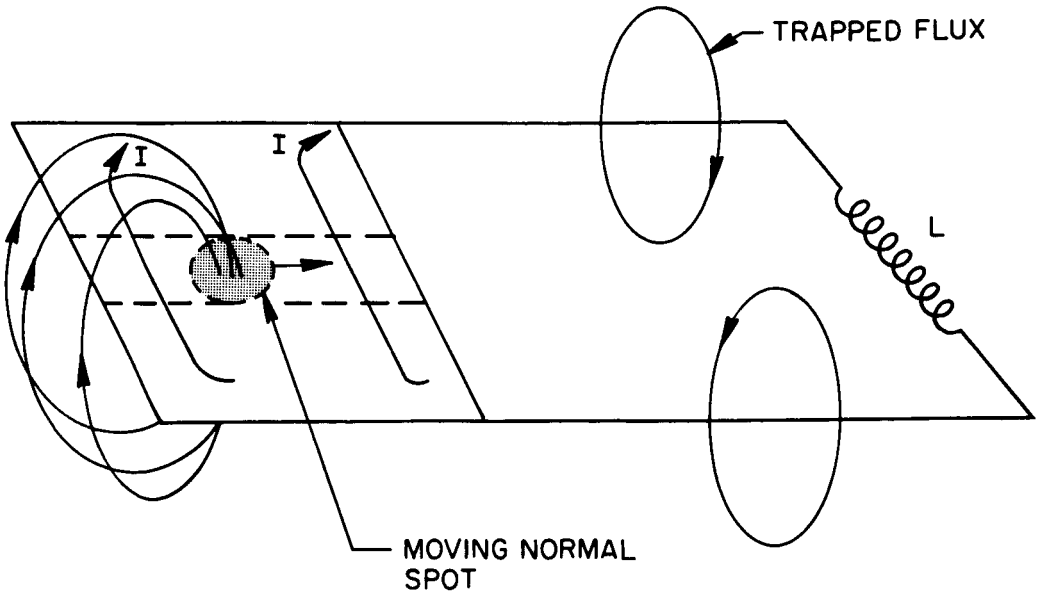

Fig. 18a Schematic arrangement for an energizer employing a moving normal region for introducing flux.

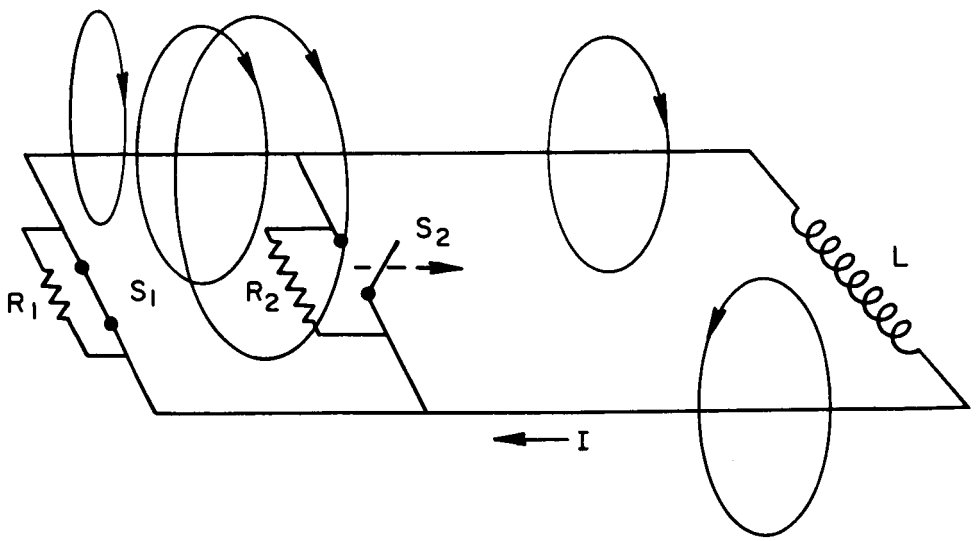

Fig. 18b Schematic arrangement for an energizer employing sequentially operated switches for introducing flux.

A5312

because in order to effect the actual transfer of the flux a transformer or other device will be needed and this will inevitably have losses.

In view of the low temperature environment it is not the actual electrical efficiency that is of prime importance. The dominant factor here is the actual helium boil-off resulting from these losses. This can vary by orders of magnitude depending upon the temperature at which the electrical losses are generated and extracted. As an example of this fact, one Joule generated at $4.2^{\circ}K$ boils off 4.63×10^{-2} gms of helium whereas one Joule at $300^{\circ}K$ boils off 2.76×10^{-4} gms. In the latter case the heat capacity as well as the latent heat of vaporization is used. It is of prime importance therefore in any flux pump application to pick a configuration in which the losses can be extracted at a high temperature.

This fact is illustrated by the comparison shown in Fig. 19. Two energizing systems are compared there, one a conventional full wave rectifier fed in with heavy leads and the other a simple transformer type flux pump. Electrically they are equivalent. The only real difference between them is the fact that one operates at room temperature and the other operates at $4.2^{\circ}K$. The losses in the switches (diodes) of the room temperature rectifier unit are insignificant only because they are generated at room temperature instead of at $4.2^{\circ}K$. At first this seems trivial because the gains that are realized by placing the rectifier at room temperature tend to be wiped out by the conduction losses of the heavy leads. However, when one stops to consider that it might be possible to operate the switches of the flux pump also at high temperature, it is no longer trivial. This is in fact a distinct possibility if the switches are properly designed.

Such a design is illustrated in Fig. 20. This unit is similar in many respects to the vapor cooled leads analyzed by Williams[17] and now used extensively for energizing large magnets from external supplies. It consists of many small diameter superconducting wires all connected in parallel and braided loosely together to form a conductor which has a large ratio of cooled perimeter to cross section. This conductor is situated inside a small dewar and the whole unit is submerged beneath the helium level inside the magnet dewar. During persistent operation the small dewar is filled with liquid helium and the switch is in the superconducting or "closed" state. Operation in the normal or "open" state is initiated by a small local heat pulse and then maintained by applying a charging voltage to the terminals below. The Joule heating produced by the charging voltage is absorbed in three ways.

1) In the latent heat of vaporization of the liquid helium
2) In the heat capacity of the resulting helium vapor
3) In the heat capacity of the resistor itself

In the analysis that follows we shall consider two limiting cases. The first is applicable to flux pumps where each charging cycle is short compared to the thermal time constant of the resistor. In this case we shall assume that the unit operates adiabatically during the time that the charging voltage is

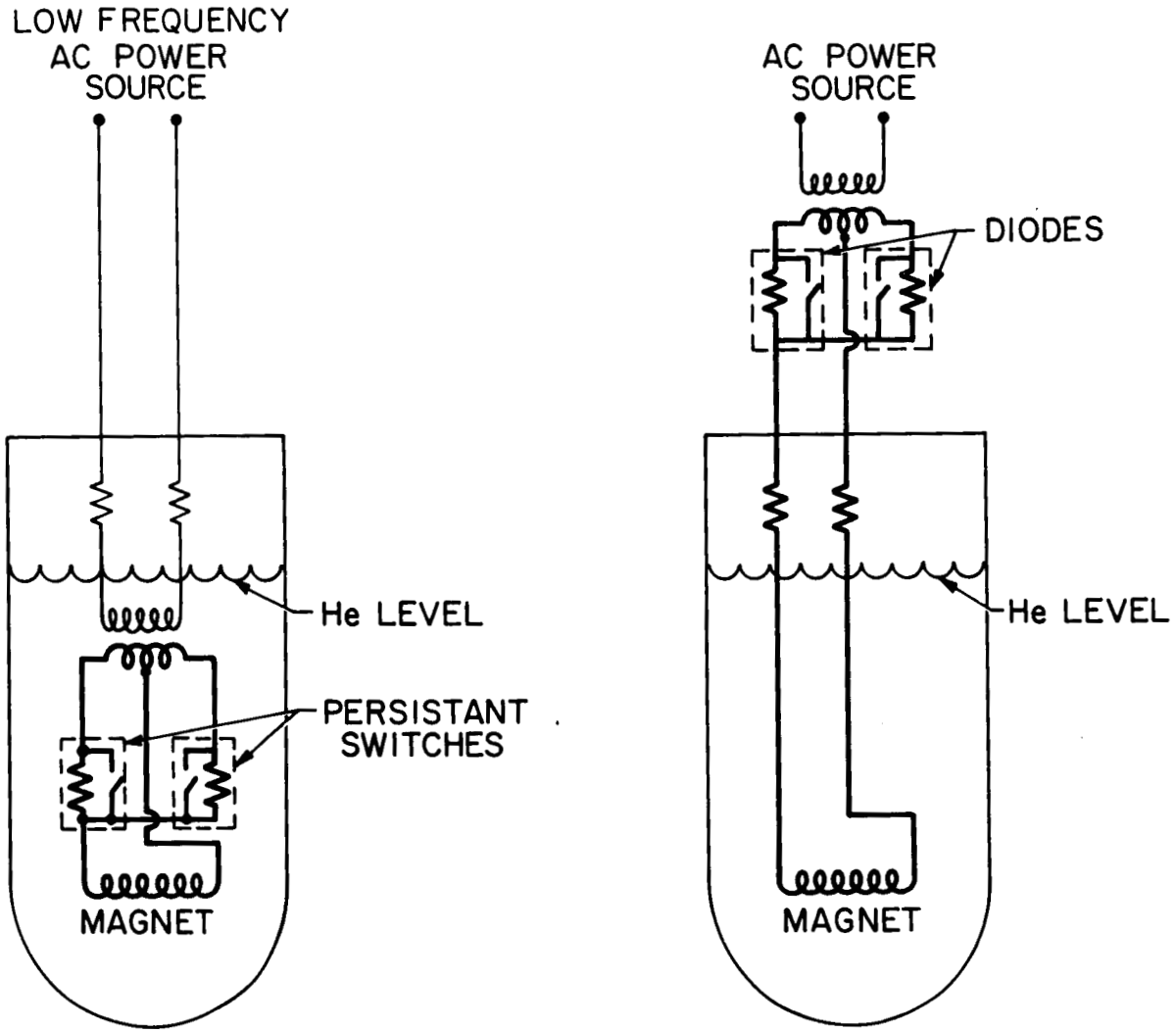

Fig. 19 Comparison of a Transformer Type Superconducting Energizer with a Conventional Full Wave Rectifier Type Power Supply. Electrically the two systems are identical, the only difference being the temperature at which the various components operate.

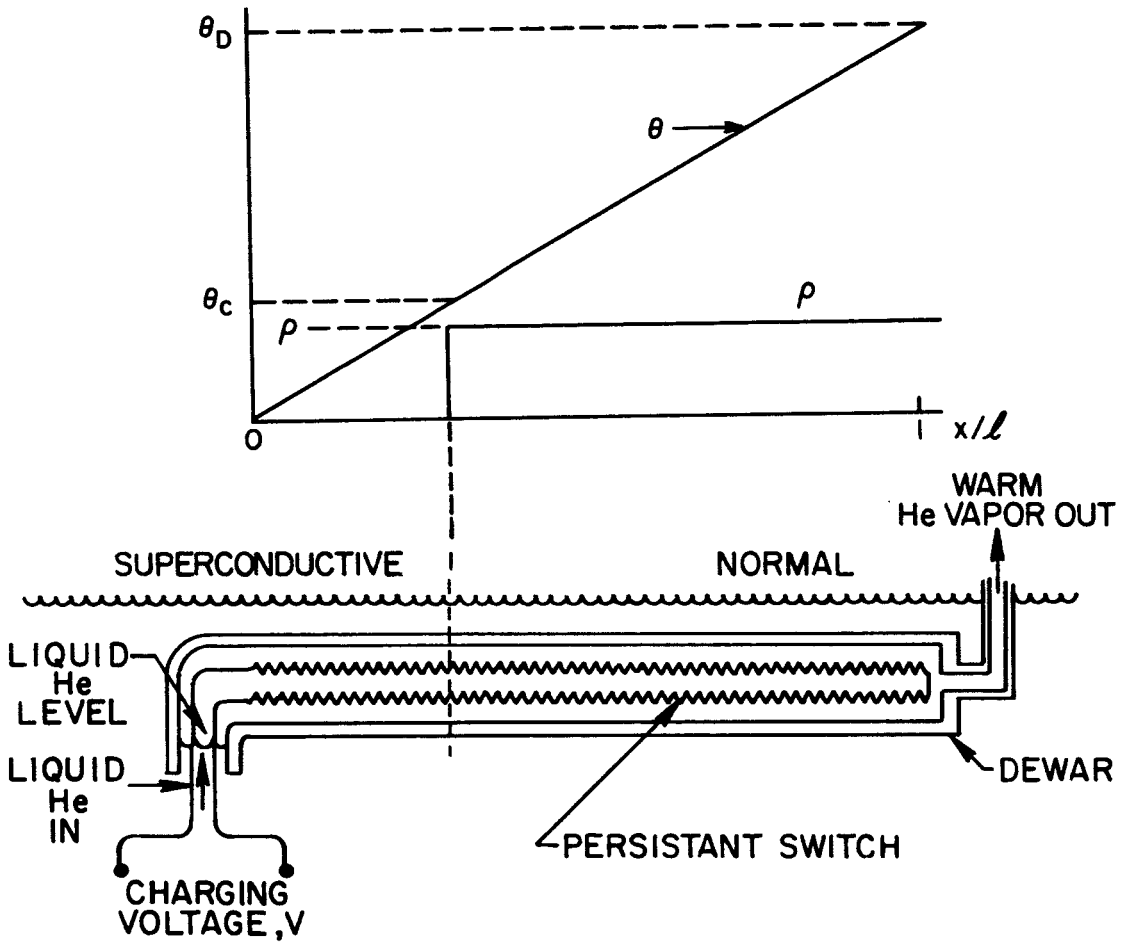

Fig. 20 Schematic arrangement of vapor cooled persistent switch for use with the transformer type energizer.

applied and is cooled during the remainder of the cycle by allowing the hot helium vapor to escape out the top while liquid helium enters at the bottom.

The second case is applicable where the charging cycle is long compared to the thermal time constant so that a steady state analysis can be used. In this case the unit operates continuously by balancing the exit vapor pressure with the charging voltage so as to maintain the liquid level at the bottom of the resistor. The heat flux appearing at the lower end then boils off just enough helium to cool to the resistor and the vapor exits at the maximum temperature occuring at the top.

Three classes of energizing schemes will be considered:

1. A flux pump
2. An externally energized magnet with vapor cooled leads
3. A magnet energized through vapor cooled leads but operated in the persistent mode by means of a vapor cooled persistent switch

These energizing schemes involve three basic components:

1. The vapor cooled persistent switch
2. The vapor cooled leads
3. The transformer

Each of these three components will be analyzed in terms of their specific boiloff, i. e. the total number of liters of helium boiled off during an experiment divided by the energy stored in the magnet. This provides a meaningful common denominator by which widely warying systems can be compared.

Adiabatic Persistent Switch

An approximate analysis of the persistent switches in their adiabatic mode can be made in terms of the following assumptions.

1. During the charging pulse, they operate adiabatically so that all energy dissipated in them goes into the heat capacity of the metal from which they are constructed.
2. During the remainder of the cycle they are cooled by helium boil-off vapor in such a way that the vapor exits at the maximum temperature of the resistor at any given time.
3. The temperature varies linearly with distance between the hot and cold ends of the resistor.
4. The heat capacity varies linearly with temperature.
5. The resistivity is finite and uniform above the critical temperature and zero below the critical temperature.
6. All temperatures are referred to bath temperature and are defined as the difference between the actual temperature and the bath temperature.

These assumptions are summarized in Fig. 20 where the temperature, heat capacity, and resistivity are plotted as a function of distance along the resistor. As illustrated there, the temperature is given by

$$\theta = \theta_d \zeta$$

where $\zeta = \frac{x}{\ell}$

x = distance from cold end (cm)

ℓ = length from cold to hot end (cm)

θ_d = temperature difference at hot end

The heat capacity if given by

$$c = C_s \frac{\theta}{\theta_r}$$

where C_s = heat capacity at 300°K ($\frac{\text{Joules}}{\text{gm°K}}$)

θ_r = room temperature difference (°K)

The resistivity is

$$\rho = \begin{cases} \rho & \theta \geq \theta_c \\ 0 & \theta < \theta_c \end{cases}$$

where θ_c = critical temperature difference (°K).

The Joule heating energy generated in the resistor during the charge cycle by a constant charging voltage, V, is

$$\mu_{rv} = \frac{V^2 \, a \, T_c \, T_p}{2\rho\ell \left(1 - \frac{\theta_c}{\theta_d} \quad N\right)}$$

where a = cross section of resistor (cm^2)

N = total number of charging cycles

T_c = total charging time

T_p = fraction of charging cycle time during which resistor is energized

Since this charging voltage is also energizing the magnet the above relation can also be expressed in terms of the total stored energy, E_s, in the

magnet. During each charge cycle, an amount of flux, $V T_c T_p/N$ is introduced into the magnet. Therefore:

$$V T_c T_p = LI = \sqrt{2 E_s L}$$

$$V^2 = \frac{2 E_s L}{T_p^2 T_c^2}$$

$$\mu_{rv} = \frac{E_s L_a}{\rho \ell N T_p T_c \left(1 - \frac{\theta_c}{\theta_d}\right)}$$

In order to trigger the switch initially a small amount of energy must be introduced by means of an auxiliary heat pulse:

$$Q_h = f \gamma_s d a C_s \frac{\theta_c^2}{\theta_r}$$

where

f = constant factor to account for the efficiency of heat transfer from the auxiliary heater to the switch wire

d = diameter of switch wire (cm)

γ_s = density of switch wire (gm/cm^3)

This amount of heat is just enough to raise a small length, d, of the resistor up to its critical temperature, thereby triggering it (it is assumed here that the minimum length that can be heated is approximately equal to the diameter, d).

The total energy released into the resistor during each cycle is then:

$$\mu_r = \frac{E_s L a}{\rho \ell N T_p T_c (1 - \frac{\theta_c}{\theta_d})} + f \gamma_s d a C_s \frac{\theta_c^2}{\theta_r}$$

Because of the assumption that the resistor operates adiabatically during the energized portion of its cycle, this energy, μ_r must all be stored in the heat capacity of the resistor.

Therefore:

$$\mu_r = 2\int_o^l \frac{\gamma_s a C_s \theta_d^2 x^2}{\theta_r \ell^2} dx = \frac{2\gamma_s a C_s \ell \theta_d^2}{3\theta_r}$$

$$\frac{2\gamma_s a C_s \ell \theta_d^2}{3\theta_r} = \frac{E_s L a}{\rho \ell N T_p T_c (1 - \frac{\theta_c}{\theta_d})} + f \mu d a c_s \frac{\theta_c^2}{\theta_r}$$

$$(\phi^2 - q)(\phi - 1) = \beta\phi$$

where $\phi = \frac{\theta_d}{\theta_c}$

$$q = \frac{3 f d}{2\ell}$$

$$\beta = \frac{3 E_s L \theta_r}{2\rho\ell^2 N T_p T_c \gamma_s C_s \theta_c^2}$$

This expresses the maximum temperature of the resistor in terms of the energy in the magnet and the charging time. It has been plotted in Fig. 21 where β is given as a function of ϕ with q as a parameter.

In order to obtain the boil-off, it is assumed that during the de-energized portion of the charging cycle the heat in the resistor is transferred to the helium vapor with 100% efficiency so that the vapor exits at the maximum temperature of the resistor. Then the boil-off, m_N, is given

$$\Delta m_N = \frac{1}{C_L + \theta C_p} \frac{\partial \mu_r}{\partial \theta} \Delta\theta = \frac{4\gamma a C_s \ell \theta \Delta\theta}{3(C_L + \theta C_p)\theta_r}$$

$$m_N = \int_O^{\theta_d} \frac{4\gamma a C_s \ell \theta d\theta}{3(C_L + \theta C_p)\theta_r}$$

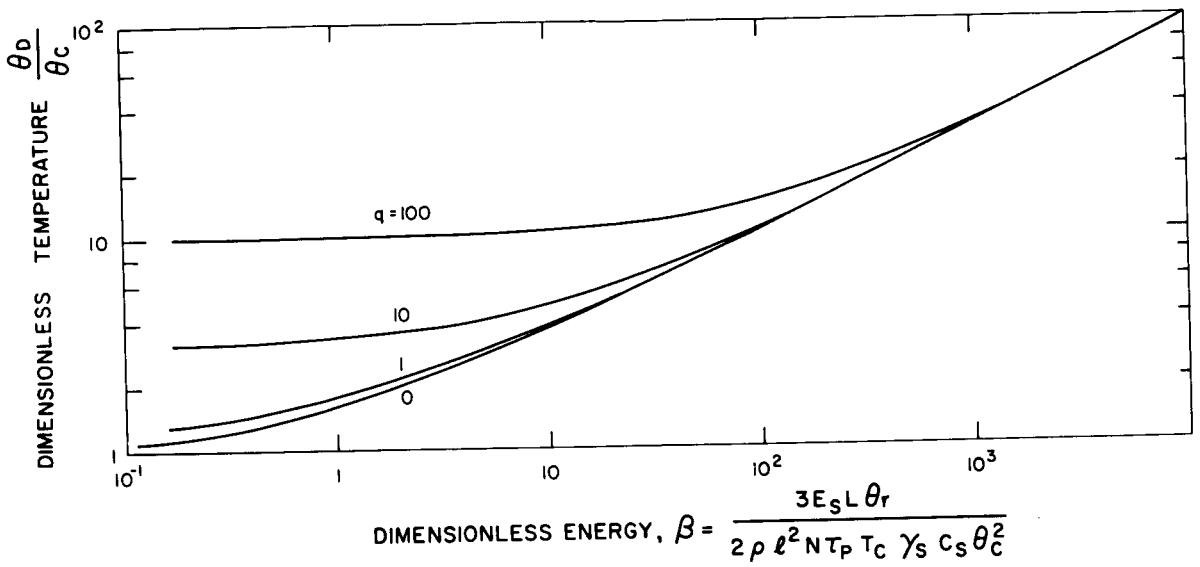

Fig. 21 Maximum Temperature of the Persistent Switch Resistor vs the Energy Parameter β

where C_L = latent heat of vaporization for helium ($\frac{\text{Joules}}{\text{liter}}$)

C_p = specific heat of helium ($\frac{\text{Joules}}{\text{liter } ^oK}$)

This is the boil-off per cycle for one of the persistent switches. Since there are necessarily two switches, the total boil-off per cycle is

$$2m_N = \frac{q\gamma a \ell C_s C_L}{3\theta_r C_p^2} \left[1 + \frac{C_p \theta_d}{C_L} - \ln\left(1 + \frac{C_p \theta_d}{C_L}\right)\right]$$

For purposes of comparing different charging systems it is useful to calculate the specific boil-off. This is defined as the total boil-off in liters of liquid helium incurred in charging a magnet to an energy E_s, divided by that energy. Thus

$$M = \frac{2 m_N N}{E_s}$$

Using the above expression for m_N and substituting for β as given in Fig. 21, the specific boil-off can be written in terms of the maximum temperature, ϕ

$$M = \frac{aL}{\rho \ell T_p T_c \gamma_{He} C_L} \frac{4\phi \left[1 + \frac{\phi}{Q_c} - \ln\left(1 + \frac{\phi}{Q_c}\right)\right] Q_c^2}{(\phi^2 - q)(\phi - 1)}$$

where $Q_c = \frac{C_L}{C_p \theta_c}$

γ_{He} = density of liquid helium

If the resistors are liquid cooled, the boil-off can be obtained from the above expression by allowing C_p to approach zero. This results in:

$$M = \frac{aL}{\rho \ell T_p T_c \gamma_{He} C_L} \frac{2Q^3}{(Q^2 - q)(Q - 1)}$$

Since the temperature is in general unknown it is more useful to express the boil-off in terms of the energy parameter β rather than the temperature. This cannot be done in closed form but can be plotted graphically as shown in Fig. 22 where the specific boil-off, M, and the temperature are shown for both vapor cooled and liquid cooled units. Three values of the trigger heat pulse parameter, q, are shown for each case in order to emphasize the consequences of over-triggering. At the lower energies this can raise the specific boil-off by orders of magnitude.

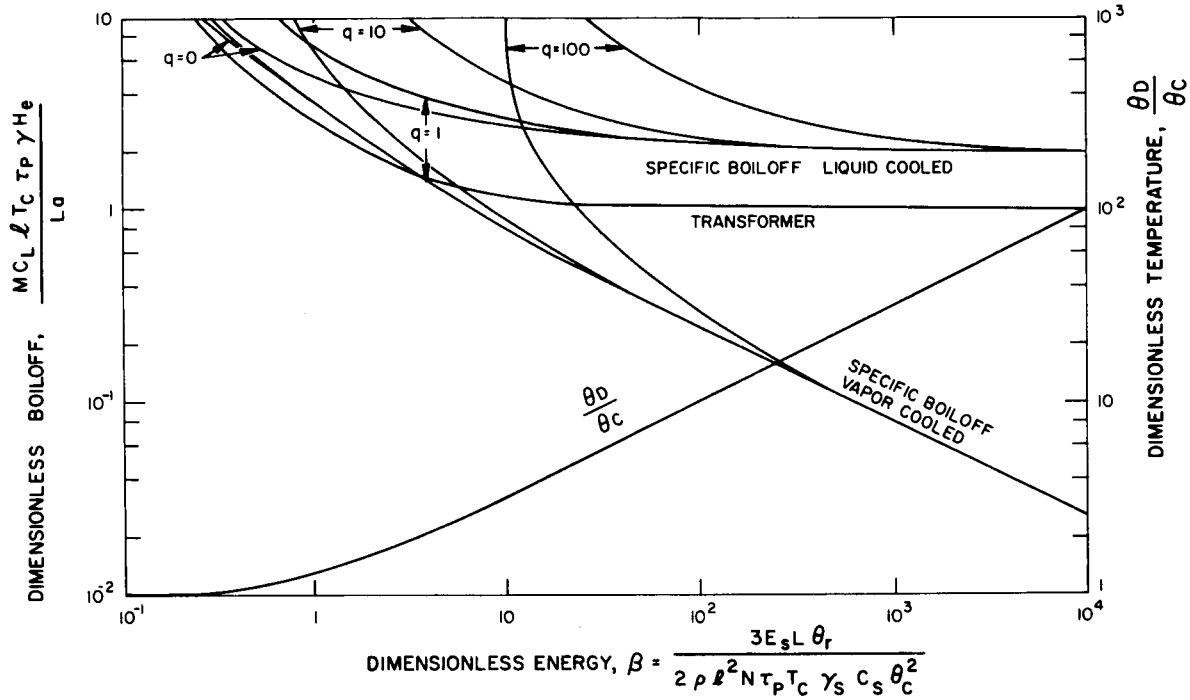

Fig. 22 Maximum Temperature and Specific Boiloff for the Persistent Switch vs the Energy Parameter β

A5211

The Transformer

The losses from the transformer section of the energizer cannot be readily extracted by vapor cooling as in the case of the persistant switches and can therefore result in a considerable portion of the total boil-off. To investigate these without going into a detailed analysis we shall simply calculate them in terms of an assumed transformer efficiency denoted by:

$$\eta = \frac{P_{out}}{P_{loss} + P_{out}} = \frac{1}{1 + \frac{P_\ell}{P_o}}$$

so that the power lost in the transformer is

$$P_\ell = P_o \left(\frac{1}{\eta} - 1\right)$$

The output power, P_o, here is the total power output including not only that which ultimately becomes stored in the magnet but also that dissipated in the persistent switches. The latter has already been calculated as:

$$2\mu_r = \frac{2E_s\, La}{\rho \ell N \tau_p T_c \left(1 - \frac{1}{\phi}\right)}$$

where ϕ is obtained from Fig. 21 in terms of the energy parameter β. The total output power of the transformer is thus:

$$P_o = \frac{2\mu_r N + E_s}{T_c}$$

and the specific boil-off for the transformer is:

$$M_t = \frac{P_\ell T_c}{E_s C_L \gamma_{He}} = \frac{La \left(\frac{1}{\eta} - 1\right)}{\rho \ell T_p C_L \gamma_{He} T_c} \quad \frac{2\phi}{\phi - 1} + \frac{\rho \ell T_p T_c}{L_a}$$

This is shown also in Fig. 22 where it is plotted as a function of β for a typical case in which

$$\eta = 0.99$$

$$\frac{\rho \ell T_p T_c}{L_a} = 100$$

The comparisons illustrated in Fig. 22 among the various boil-off components of a transformer type energizer, point out several important facts with regard to their design.

1. If vapor cooling is used the boil-off for the persistant switches can generally be lowered to the point where the design emphasis should be on the transformer efficiency rather than that of the switches.

2. The trigger heat pulse should be only large enough to initiate a small normal region which can be enlarged later by the application of the charging voltage. Over-triggering can result in serious unnecessary boil-off particularly at lower values of β. This is true whether or not vapor cooling is used.

3. For values of β greater than unity the charging time has little effect on the boil-off. For short charging times the electrical efficiency is poorer but the extra loss energy all goes into raising the exit helium vapor temperature rather than boiling off more liquid.

The Steady State Persistent Switch

The steady state analysis of the persistent switch will follow closely Williams' analysis of vapor cooled leads. Basically it is the same device, the only difference being in the character of the electrical resistivity and the manner it is connected into the circuit. The model to be analyzed is shown in Fig. 23 and it consists of a resistor made of superconducting material arranged in such a way as to provide a large ratio of cooled perimeter to cross section so that its temperature essentially equals that of the vapor at each point along its length. The resistor is placed inside a small dewar and the entire unit is submerged beneath the helium liquid level. In the persistent mode the unit is filled with liquid helium and serves as a zero resistance short on the magnet. Operation in the charging or "normal" mode is started by applying a triggering heat pulse at the top end and allowing the resulting boil-off to force the liquid out of the small dewar surrounding the resistor. Steady state operation in the charging mode is maintained by balancing the charging voltage and the exit helium vapor pressure so that the liquid level inside the unit remains at the lower end of the resistor. The heat flux appearing at the bottom end then provides just enough boil-off to cool the resistor and the temperature at the upper end depends only on the charging voltage applied and the resistance.

A steady state analysis will be performed, neglecting the initial trigger pulse and all heat capacity effects. The thermal conductivity will be assumed independent of temperature and the electrical resistivity will be assumed zero below the critical temperature and independent of temperature above the critical temperature. With these assumptions the following equilibrium equations can be written in terms of the temperature difference, θ existing between the bath temperature and the temperature at a distance x down from the top.

$$\frac{\partial^2 \theta_1}{\partial \zeta^2} + \frac{C_p m \ell}{Ka} \frac{\partial \theta_1}{\partial \zeta} \frac{\rho \ell^2 \zeta_c^2 I_R^2}{Ka^2} = 0 \qquad 0 < \zeta < \zeta_c$$

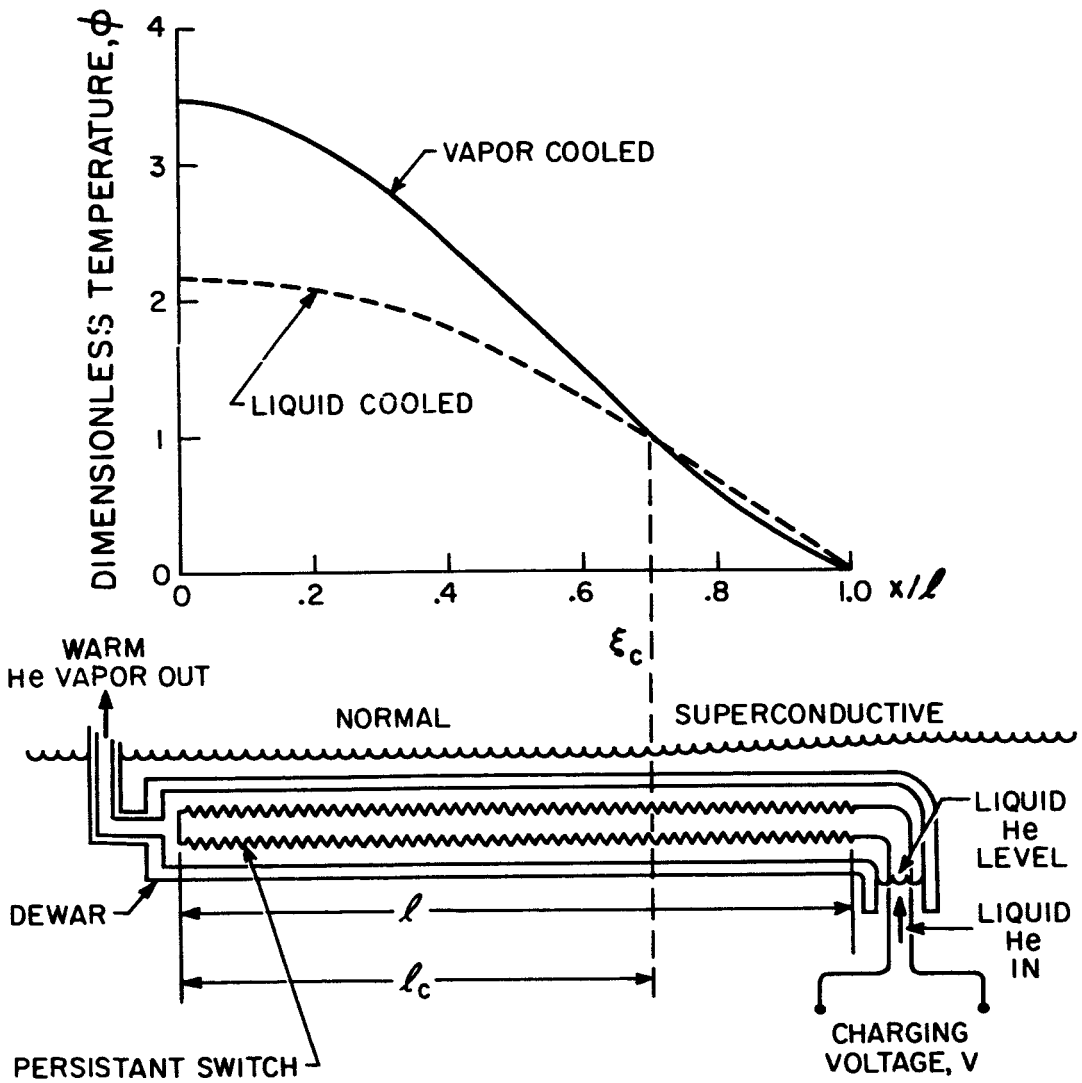

Fig. 23 Schematic Arrangement of the Vapor Cooled Persistent Switch when Operated in Steady State

and

$$\frac{\partial^2 \theta_2}{\partial \zeta^2} + \frac{C_p m \ell}{Ka} \frac{\partial \theta_2}{\partial \zeta} = 0 \qquad \zeta_c < \zeta < 1$$

where:

θ = temperature difference between the resistor and the bath (^oK)

ζ = x/ℓ

ℓ = length of resistor between hot and cold end

m = helium vapor flow rate ($\frac{gm}{sec}$)

C_p = helium vapor heat capacity (Joules/gm ^oK)

K = thermal conductivity of resistor ($\frac{Joules}{sec\ cm\ ^oK}$)

a = cross section of resistor (cm^2)

ρ = resistivity of resistor (Ω cm)

I_R = current in resistor (A)

x_c = distance to transition point (cm)

θ_c = critical temperature difference (^oK)

The boundary conditions are:

1. At the top ($x = 0$) the gradient vanishes
2. At $x = x_c$ the temperature is critical ($\theta = \theta_c$) and the gradient is continuous
3. At the bottom ($x = \ell$) the temperature difference is zero, and the temperature gradient results in the boil-off which cools the lead, i. e.

$$\frac{Ka}{\ell} \frac{\partial \theta_2}{\partial \zeta} \Bigg|_{\ell} = - m C_L$$

where C_L = latent heat of vaporization (Joules/gm).

Then the temperature at any point on the resistor is

$$\theta_1 = \theta_c \left[\frac{(Q_c + 1)\left[1 - e^{-A\zeta} + A(\zeta_c - \zeta)\right]}{1 - e^{-A\zeta_c}} - Q_c \right]$$

and

$$\theta_2 = \theta_c Q_c \left[e^{-A(\zeta - 1)} - 1 \right]$$

where:

$$A = \frac{m C_p \ell}{Ka}$$

The relationship between the parameters A and ζ_c is given by two equations.

$$A = \frac{\ell n \left(1 + \frac{1}{Q_c}\right)}{1 - \zeta_c}$$

$$B = \frac{(Q_c + 1)\, \zeta_c^2\, A^2}{1 - e^{-A \zeta_c}}$$

where

$$B = \frac{\rho \ell^2 \zeta_c^2 I_r^2}{K a^2 \theta_c}$$

Elimination of ζ_c between these two equations then results in the relation shown in Fig. 24 between the boil-off parameter A and the current parameter B. In order to obtain the specific boil-off in a way which can be related to the energy stored in the magnet it is necessary to write the parameters A and B in a slightly different form. This is the form shown in Fig. 24 and it is derived as follows:

The current I_r in the resistor is given by:

$$I_r = \frac{V_a}{2 \rho x_c}$$

The total energy in the magnet after a charging time T_c is

$$E_s = \frac{L I_L^2}{2} = \frac{V^2 T_c^2}{2 L}$$

Therefore:

$$I_r = \frac{a \sqrt{2 E_s L}}{2 T_c \rho x_c}$$

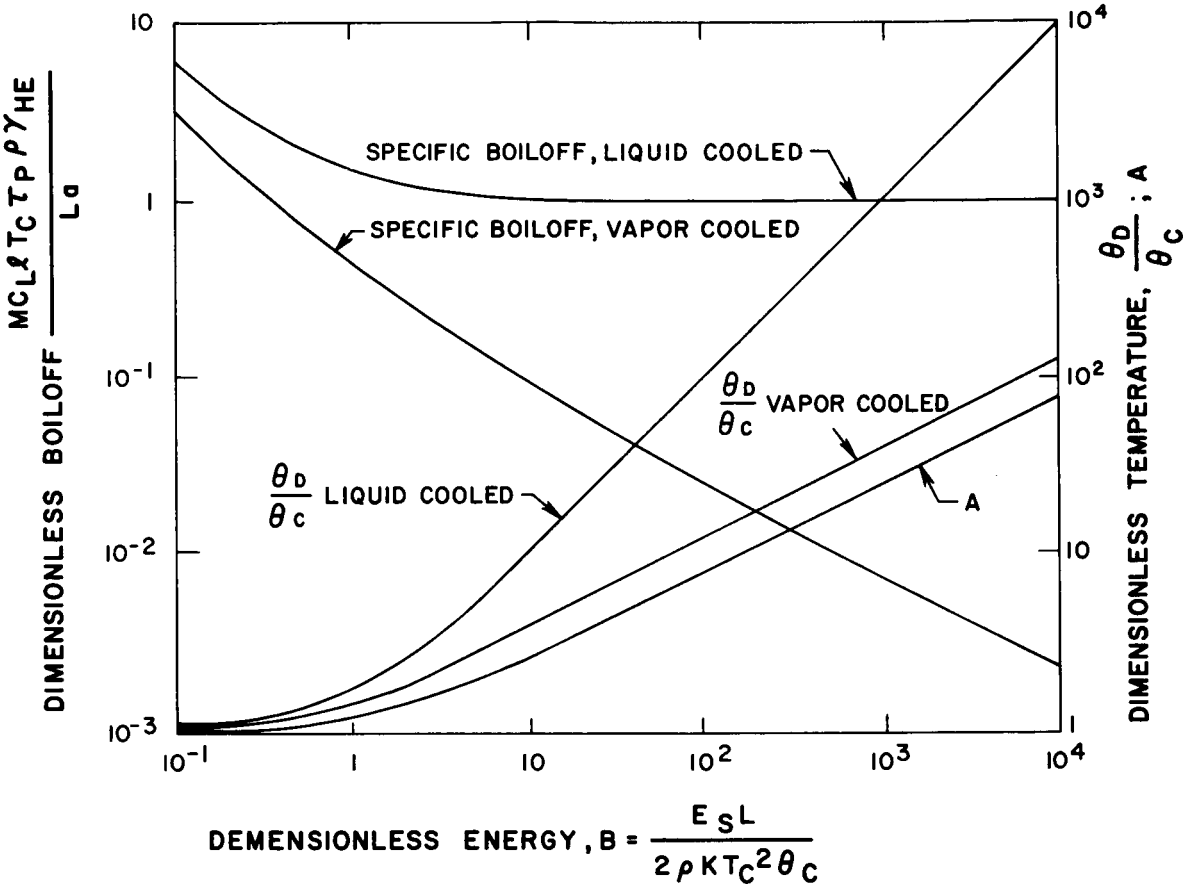

Fig. 24 Maximum Temperature and Specific Boiloff for the Persistent Switch Operated in Steady State

A5214

and

$$B = \frac{E_s L}{2K T_c^2 \rho}$$

The specific boil-off is obtained from the ratio of A to B.

$$\frac{A}{B} = \frac{2 m T_c^2 C_L \ell \rho}{a L E_s}$$

$$M = \frac{m T_c}{E_s \gamma_{He}} = \frac{A Q_c a L}{2 B C_L \ell T_c \rho \gamma_{He}}$$

This is also plotted in Fig. 24.

The maximum temperature is given by:

$$\theta_1 \Big|_{\zeta = 0} = \theta_c \left[\frac{(Q_c + 1) A \zeta_c}{1 - e^{-A \zeta_c}} - Q_c \right]$$

$$= \theta_c \left[\left(\frac{1}{\frac{A}{B} - \frac{\ell n (1 + 1/Q_c)}{B}} \right) - Q_c \right]$$

and is also plotted in Fig. 24.

Using the data in Fig. 24 the specific boil-off can also be plotted as a function of maximum temperature as shown in Fig. 25. This shows directly the advantage to be gained by fully utilizing the heat capacity of the vapor.

If the persistent switch is liquid cooled only, (i.e. the boil-off vapor is extracted at the bath temperature) the equilibrium equations are:

$$\frac{\partial^2 \theta_1}{\partial \zeta^2} + \frac{B \theta_c}{\zeta_c^2} = 0 \qquad 0 < \zeta < \zeta_c$$

and

$$\frac{\partial^2 \theta_2}{\partial \zeta^2} = 0 \qquad \zeta_c < \zeta < 1$$

Using the same boundary conditions as with the vapor cooled case, the solutions are:

$$\theta_1 = \frac{\theta_c}{1 - \zeta_c} \left[1 - \frac{\zeta_c}{2} - \frac{\zeta^2}{2\zeta_c}\right] \qquad 0 < \zeta < \zeta_c$$

$$\theta_2 = \theta_c \left(\frac{1 - \zeta}{1 - \zeta_c}\right) \qquad \zeta_c < \zeta < 1$$

where

$$\zeta_c = \frac{B}{\frac{1}{2} + B}$$

The specific boil-off is given by:

$$M = \frac{La}{C_L \ell T_c \rho \gamma_{He}} \left[1 + \frac{1}{2B}\right]$$

and the maximum temperature is

$$\theta_D = \theta_c (1 + B)$$

These quantities have been plotted in Fig. 24 for comparison with the vapor cooled case.

The specific boil-off can also be expressed in terms of the maximum temperature:

$$M = \frac{1}{2 C_L \gamma_{He} \ell \rho T_c a L} \left[\frac{\phi - \frac{1}{2}}{\phi - 1}\right]$$

This has also been plotted in Fig. 25 for comparison with the vapor cooled case.

Comparison of Componets

In order to make a meaningful appraisal of the various charging methods available, it is useful to make some very general comparisons. In this section, therefore, we shall derive some approximate expressions with which the various components can be compared directly. To do this we shall calculate the specific boil-off for the particular charging sequence shown in Fig. 26. The magnet is started from zero energy, charging at a constant

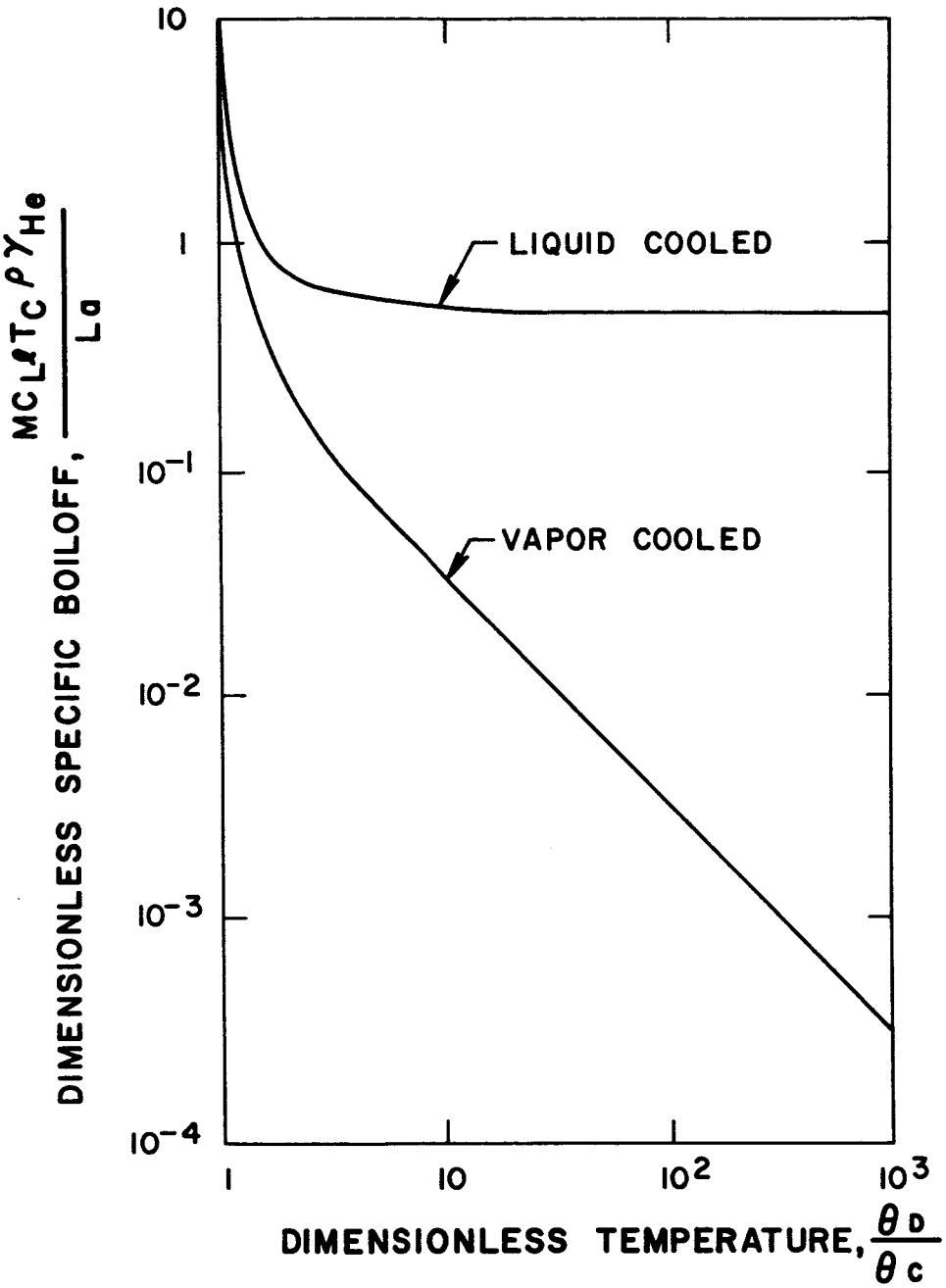

Fig. 25 Specific Boiloff for the Steady State Persistent Switch vs Maximum Temperature

A5213

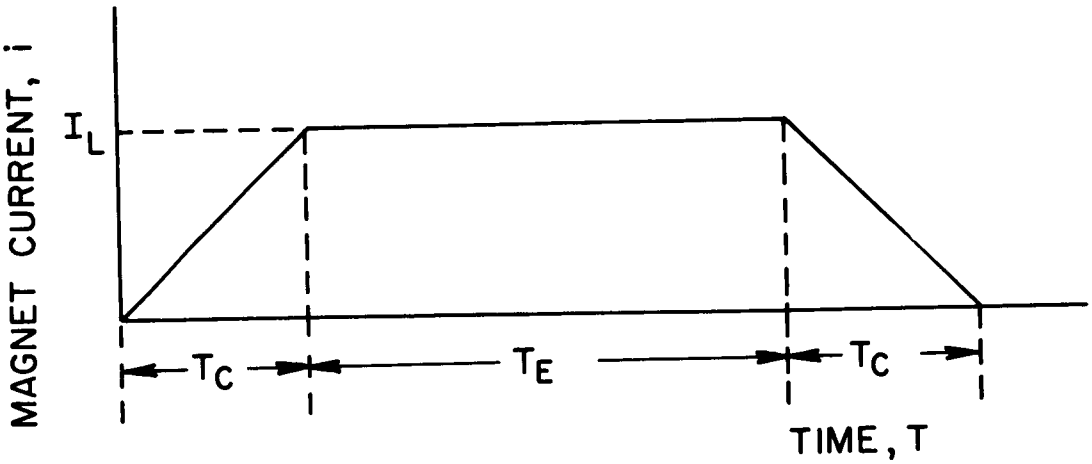

Fig. 26 Magnet Charging Sequence for Comparison of Various Energizing Schemes

voltage to an energy E_S in time T_C, then maintained constant at this level for a time T_E and finally discharged at a constant rate for a time T_C back to zero. The specific boil-off will be calculated for the following cases.

1. A transformer energizer with vapor cooled persistent switches.
2. A transformer energizer with liquid cooled persistent switches.
3. Optimum counter-flow leads.
4. Non optimum counter-flow leads with a vapor cooled persistent switch.
5. Non optimum counter-flow leads with a liquid cooled persistent switch.

While the formulas derived above are useful for obtaining the specific boil-off, once the various fundamental parameters have been specified, their usefulness for making general comparisons among types of systems is compromised by the complexity of the dimensionless parameters used. Quantities such as ℓ, T_C, and L appear on both sides of the equations making direct comparisons awkward. In the following, therefore, we shall examine the asymptotic behavior of these relationships. These are much simpler, enabling one to make more direct comparisons. Fortunately the ranges of B and β for which these approximations hold, coincide substantially with those of engineering interest.

Transformer Energizer

In the case of the transformer energizer the relationship between ϕ and β,

$$\beta \phi = (\phi - 1)(\phi^2 - q)$$

reduces to

$$\beta = \phi^2$$

for

$$\beta \gg q + 1$$

and the resulting specific boil-off is

$$M_{vc} \approx \frac{4\theta_c}{\gamma_{He} C_L Q_c J_c} \sqrt{\frac{N \gamma_s C_s}{3\rho \tau_p T_c \theta_r}}$$

for the vapor cooled case and

$$M_{Lc} \approx \frac{2\sqrt{2 E_s L}}{\rho \ell \tau_p T_c \gamma_{He} C_L J_c}$$

for the liquid cooled case. Furthermore the cross sectional area, a appearing in the boil-off parameter, A, must be such that the full current, I_L, can pass.

Thus:

$$a = \frac{I_L}{J_c}$$

where J_c = critical current density of the resistor (A/cm^2).

The boil-off for the transformer is

$$M_T \approx \frac{\left(\frac{1}{\eta} - 1\right)}{C_L \gamma_{He}} \left[1 + \frac{2\ 2\ E_s L}{J_c \rho \ell \tau_p T_c}\right]$$

These three quantities have been plotted in Fig. 27 using the following numerical values for the parameters.

$\theta_c = 6^{\circ}K$

$\gamma_{He} = 125$ gm/l

$C_L = 21.6$ J/gm

$Q_c = 0.6$

$J_c = 10^5$ A/cm^2

$\gamma_s = 8$ gm/cm^3

$C_s = 0.27$ J/gm$^{\circ}$K

$\ell = 100$ cm

$\eta = 0.99$

$\beta > 10$

$\rho = 2.54,\ 10^{-5}\ \Omega$ cm

$\tau_p = 0.5$

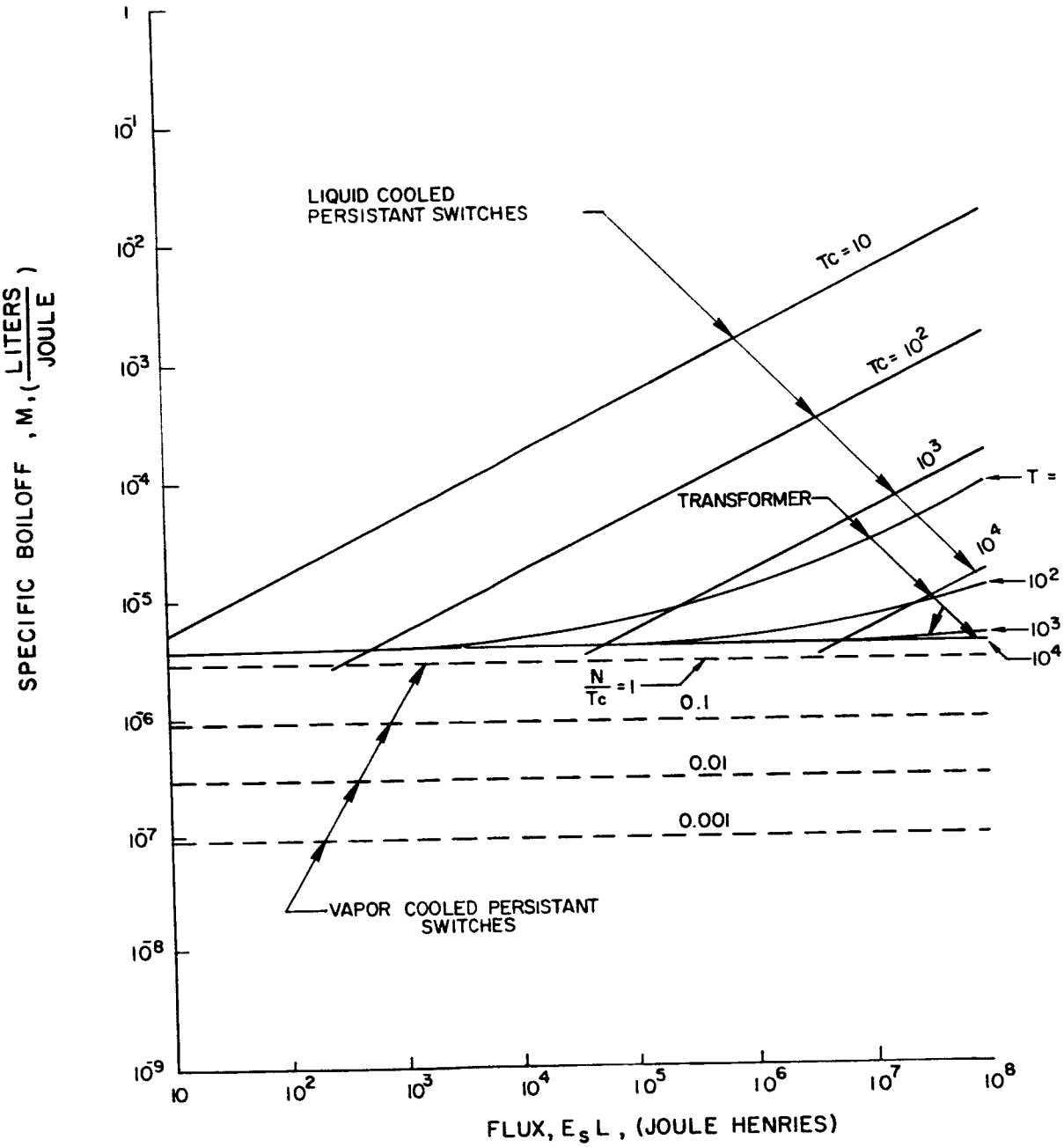

Fig. 27 Comparison of the boiloff for the various components of a transformer energizer using either liquid or vapor cooled persistent switches.

Two important facts become evident from these relationships.

1. The boil-off for vapor cooled persistent switches is independent of the energy and also independent of the length or cross section of the resistor, provided the necessary surface to cross section ratio is maintained and the temperature limitations are not exceeded.
2. For a system using vapor cooled switches the transformer is the dominant loss factor (at this efficiency at least) rather than the persistent switches. This surprising result is due mainly to the fact that the transformer cannot readily be vapor cooled.

Evidently in the development of the transformer energizer the transformer design requires at least as much attention as the persistent switch design.

Counterflow Leads

The specific boil-off for incoming leads can be obtained from Williams' analysis.[17] The boil-off there is given by two dimensionless parameters:

$$A_w = \frac{m\, c_p\, \ell_c}{a}$$

$$B_w = \frac{2\, I_L\, \ell}{a} \sqrt{\frac{a}{K_c}}$$

The parameters are all the same as those in the present analysis except that the resistivity of copper used in the leads is approximated linearly by:

$$\rho_c = a\,\theta$$

where

$$a = \frac{2}{\theta_D^{\,2}} \int_o^{\theta_D} \rho_o\ (\theta)\ d\theta$$

$\rho_o\ (\theta)$ = actual temperature variation.

A_w and B_w are related by

$$\frac{C_L}{C_p\, \theta_D} = \frac{\sqrt{B_w^{\,2} - A_w^{\,2}}\ e^{-\frac{A_w}{2}}}{2\, A_w \sin \frac{1}{2}\sqrt{B_w^{\,2} - A_w^{\,2}}}$$

If $B_w >> 1$ this relationship is satisfied if

$$A \approx B \sqrt{1 - \frac{4\pi^2}{B^2}} \approx B \left(1 - \frac{2\pi^2}{B^2}\right)$$

The specific boil-off is obtained as usual from the ratio of A_w/B_w

$$M = \frac{2 A_w}{B_w} \quad \frac{T_E}{\gamma_{He} C_p} \quad \sqrt{\frac{2 a K_c}{L E_s}}$$

where T_E is the total time during which the magnet is held at its working energy E_s. In order to simplify the analysis the boil-off during charging is approximated by taking half the boil-off rate existing at full current for the charging and discharging periods. The total specific boil-off for two leads is thus:

$$M_\ell = \frac{4 A_w}{B_w} \quad \frac{(T_E + T_c}{\gamma_{He} C_p} \quad \sqrt{\frac{2 a K}{L E_s}}$$

If they are optimum leads according to Williams:

$$\frac{A_w}{B_w} = .84$$

Therefore

$$M_{opt.} = 3.36 \quad \frac{(T_E + T_c)}{\gamma_{He} C_p} \quad \sqrt{\frac{2 a K_e}{L E_s}}$$

When a persistent switch is used it is advantageous to run the charging leads at a higher current than the optimum discussed by Williams. This results in more boil-off during the charge but less during persistent operation because the lead cross section is smaller. The extent to which this scheme can be used to reduce the overall boil-off is limited by the maximum allowable current density that can be tolerated in the leads. To obtain the specific boil-off for these non-optimum leads, we shall simply take $A_w/B_w = 1$. This is the limiting value of the ratio when A_w and B_w becomes indefinitely large. During the persistent operation the boil-off is the zero current value, which according to Williams is given by:

$$m = \frac{4.42 aK}{C_p \ell} = \frac{4.42 K}{C_p \ell J_e} \sqrt{\frac{2 E_s}{\ell}}$$

The specific boil-off for the charging and discharging periods is thus:

$$\frac{m\ T_c}{E_s\ \gamma_{He}} = \frac{4.42\sqrt{2}\ T_c\ K}{C_p \ell\ J_e\ \gamma_{He}\sqrt{E_s L}}$$

Thus the total for the leads is

$$M_\ell = \frac{4\ T_c}{\gamma_{He} C_p}\sqrt{\frac{2\ a\ K}{L E_s}} + \frac{8.6\ K\ T_E}{\ell\ C_p\ \gamma_{He}\ J_e}\sqrt{\frac{2}{E_s L}}$$

In the case of the steady state persistent switch for use with these leads the boil-off and energy parameters are related by two simultaneous equations.

$$A = \frac{\ell n\ (1 + \frac{1}{Q_c})}{1 - \zeta_c}$$

$$B = \frac{(Q_c + 1)\ S_c^{\ 2}\ A^2}{1 - e^{-AS_e}}$$

As ζ_c approaches unity A becomes much greater than unity so that

$$B \approx (Q_c + 1)\ \zeta_c^{\ 2}\ A^2$$

$$M \approx \frac{1}{J_c\ \gamma_{He}\ \ell\ C_p}\sqrt{\frac{k}{\rho\ (1 + Q_c)}}$$

This shows that the specific boil-off is independent of the energy and the charging time, depending only on the length of the resistor and the properties of the material from which it is constructed.

If the persistent switch is liquid cooled, the specific boil-off is

$$M = \frac{\sqrt{2\ E_s L}}{C_L\ \gamma_{He}\ \rho\ \ell\ T_c J_c}\left[\frac{1 + \frac{Q_c}{B}}{2}\right]$$

which reduces to

$$M = \frac{\sqrt{2\ E_s L}}{2\ C_L\ \gamma_{He}\ \rho\ \ell\ T_c J_c}$$

for $B >> Q_c$.

In Fig. 28 the specific boil-off for each of these components is plotted for comparison, using the following typical values for the parameters.

$$\ell_c = 100 \text{ cms}$$

$$a = 5\ 10^{-9}\ \Omega \text{ cm}/^{\circ}\text{K}$$

$$K_c = 4 \text{ W/cm}^{\circ}\text{K}$$

Optimum Liquid Cooled Leads

To complete the picture we also calculate the specific boil-off for a magnet energized by copper leads which have been optimized according to an analysis by McPhee[18] and not vapor cooled.

According to McPhee the ℓ/a ratio for minimum boil-off is given by

$$\frac{\ell}{a} = 5\ 10^4 \quad I_L \ (\text{cm}^{-1})$$

for a copper lead when the warm end of the lead is at 290°K and the cold end at 4.2°K. Using this value of ℓ/a the boil-off is given by

$$M = (0.042)\ C_L\ I_L$$

Then for two leads the specific boil-off is

$$M = \frac{m\ (T_c + T_E)}{E_s\ \gamma_{He}} = \frac{0.084\ \sqrt{2}\ C_L\ (T_c + T_E)}{\gamma_{He}\ \sqrt{E_s L}}$$

This expression has also been plotted in Fig. 28.

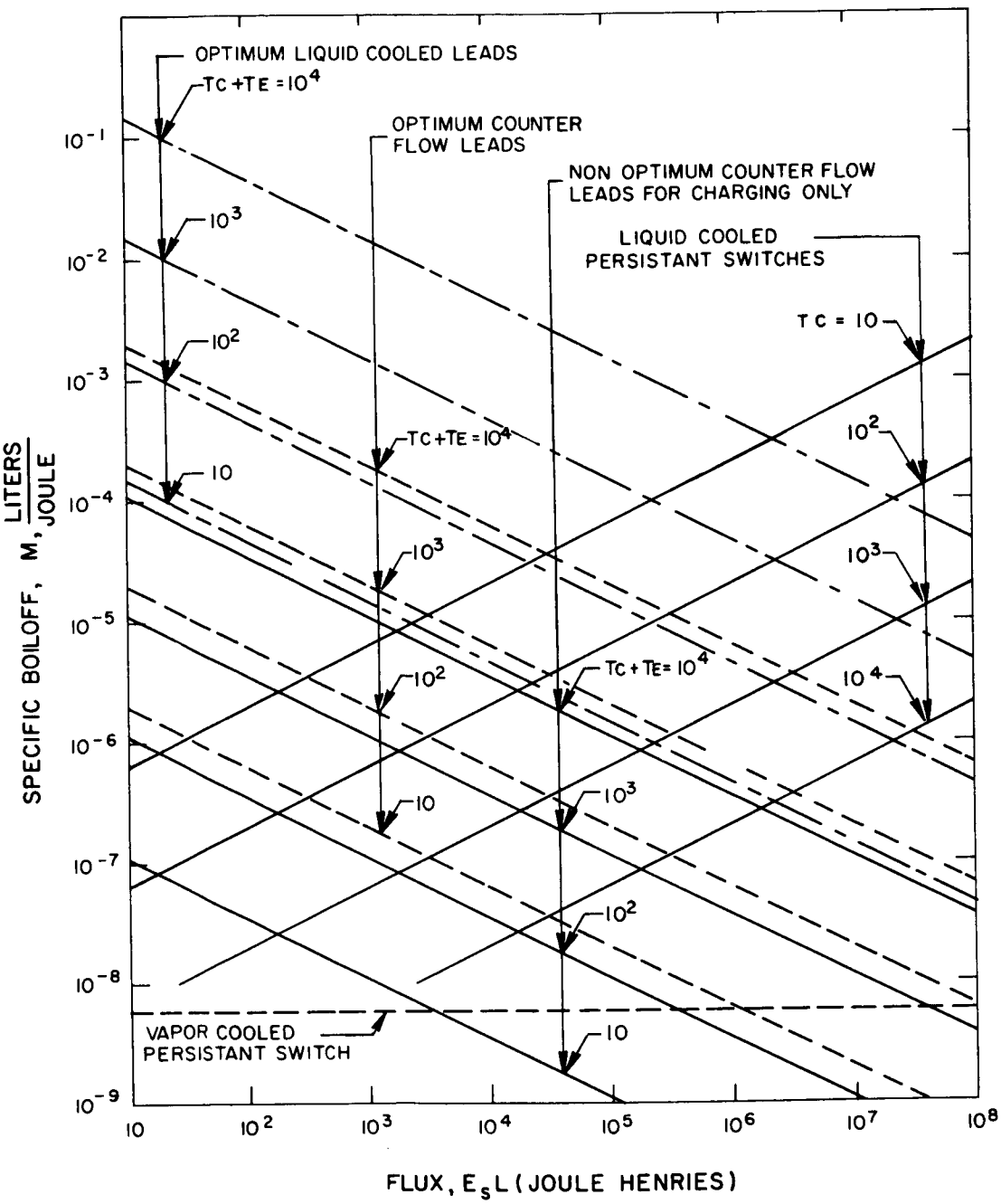

Fig. 28 Comparison of the boiloff for the various components of external energizing systems employing counter flow leads, uncooled leads and persistent switches.

A5222

VII. OPERATION OF AN EXPERIMENTAL TRANSFORMER TYPE ENERGIZER

A superconducting transformer type energizer was constructed and used to charge the 25 cm O.D. strip magnet.[19] Currents of up to 540 amps were generated resulting in a central field of 0.32 Wb/m^2. With this unit it was possible to charge and discharge the coil and operate it in the persistent mode. At 540 amperes the coil was allowed to run in the persistent mode for over an hour without any discernable decay in field. The unit employed thermally operated persistent switches in a circuit as shown in Figs. 29a and 29b. Figure 29a shows the spacial relationships of the various components, while Fig. 29b illustrates the circuit schematically in terms of circuit components.

The persistent switches were constructed as shown in Fig. 30 in the form of coils of stabilized Nb-25% Zr strip interwound with electrical insulation and a nicrome heater strip. No attempt was made to dissipate the switch energy at temperatures above 4.2° but the switches were provided with a phenolic shroud in order to approximate the conditions outlined above for liquid cooled switches. The shroud was designed so that during the normal or "open" state the boiloff vapor would drive out the liquid and provide an adiabatic situation. A sufficient length of face cooled strip was provided outside the shroud to insure that the conductor was in the superconducting state before it entered the junction with the magnet conductor.

The transformer consisted of a solid mild steel core incorporating a 360 turn superconducting primary and a single turn of stabilized Nb-25% Zr strip as the secondary.

Instrumentation was provided for measuring the following:

1) Voltage across S_1
2) Magnet terminal voltage
3) S_1 heater voltage
4) S_2 heater voltage
5) Transformer primary voltage
6) Transformer secondary voltage
7) Primary current
8) Central field

These quantities were all recorded simultaneously by means of a multichannel recording system. The timing of the primary voltage pulses

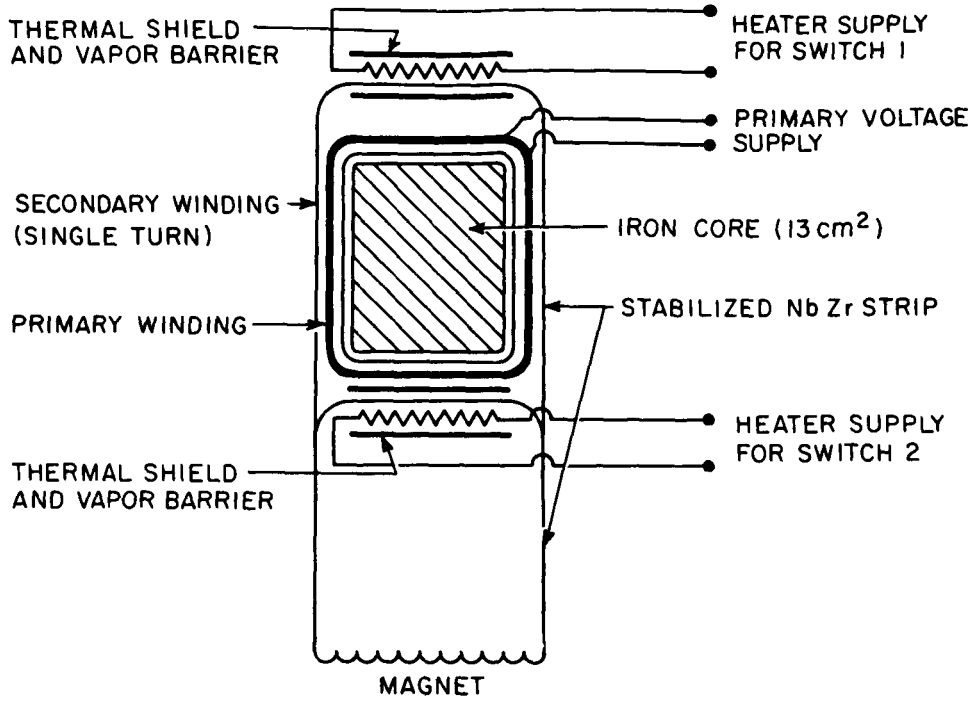

Fig. 29a Schematic Showing Spatial Arrangement of the Transformer and Switches in the Experimental Energizer

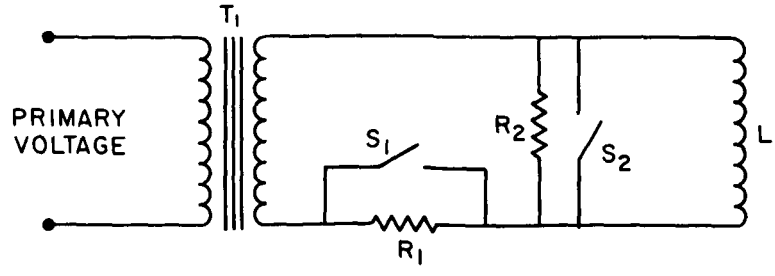

Fig. 29b Circuit Diagram for the Experimental Transformer Energizer

A5313

A5313

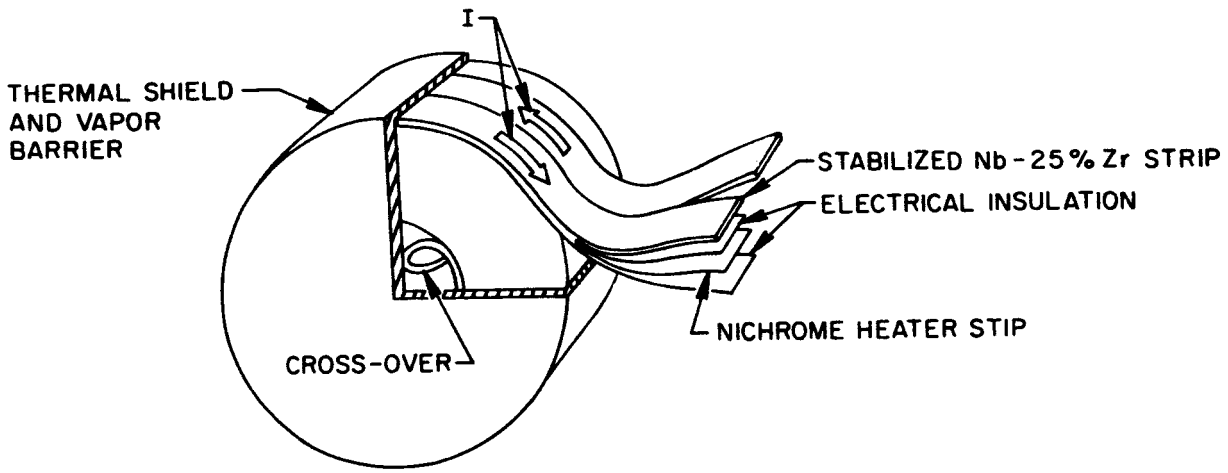

Fig. 30 Persistent Switch Construction for Liquid Cooled Units used in Experimental Transformer Energizer

and the persistent switch heater pulses was accomplished by means of cam operated switches.

Operation

Operation of the unit involved charging the 25 cm O.D. strip magnet[9] from zero to 540A in 3300 sec with a total of 450 charging cycles. The sequence of events used in the operation of the device is as follows:

1) Initially there is no current anywhere in the system

2) S-1 is opened

3) A negative voltage is applied to the primary and is allowed to remain until the transformer core is saturated in the negative direction, whereupon the voltage is removed.

4) S-1 is closed and S-2 is opened. (Note that no currents exist in either switch before or after their operation).

5) A positive voltage is applied to the primary and allowed to remain until the core is saturated in the positive direction, at which time it is removed. This introduces a total of twice the saturation flux into the coil.

6) S-2 closed. (There is now a persistent current flowing through the transformer secondary, S-1 and L, the coil being charged).

7) A reverse current is passed through the primary of such magnitude as to reduce the persistent current in S-1 to zero. This in effect transfers all the current in L from S-1 to S-2.

8) S-1 is opened.

9) A negative voltage is applied to the primary and allowed to remain until the core is negatively saturated.

In actual practice step 7 was omitted, i.e., no attempt was made to monitor the current in S-1.

A summary of the important quantities relating to the test are given in Table II and a typical example of the time variation of some of these quantities is shown in Fig. 31. A total of four complete cycles are shown there, with the last one expanded by a factor of 10 to obtain better resolution. This expanded cycle reveals the following important facts about the operation of the unit.

1) Normally one would expect to observe two charging voltage pulses per cycle, one for each change in primary current. The fact that only one exists here is due to the coercive force of the solid iron transformer core. When the primary current is returned to zero very little change in core flux takes place. The major change takes place when the primary current is reversed and the core is driven into positive saturation.

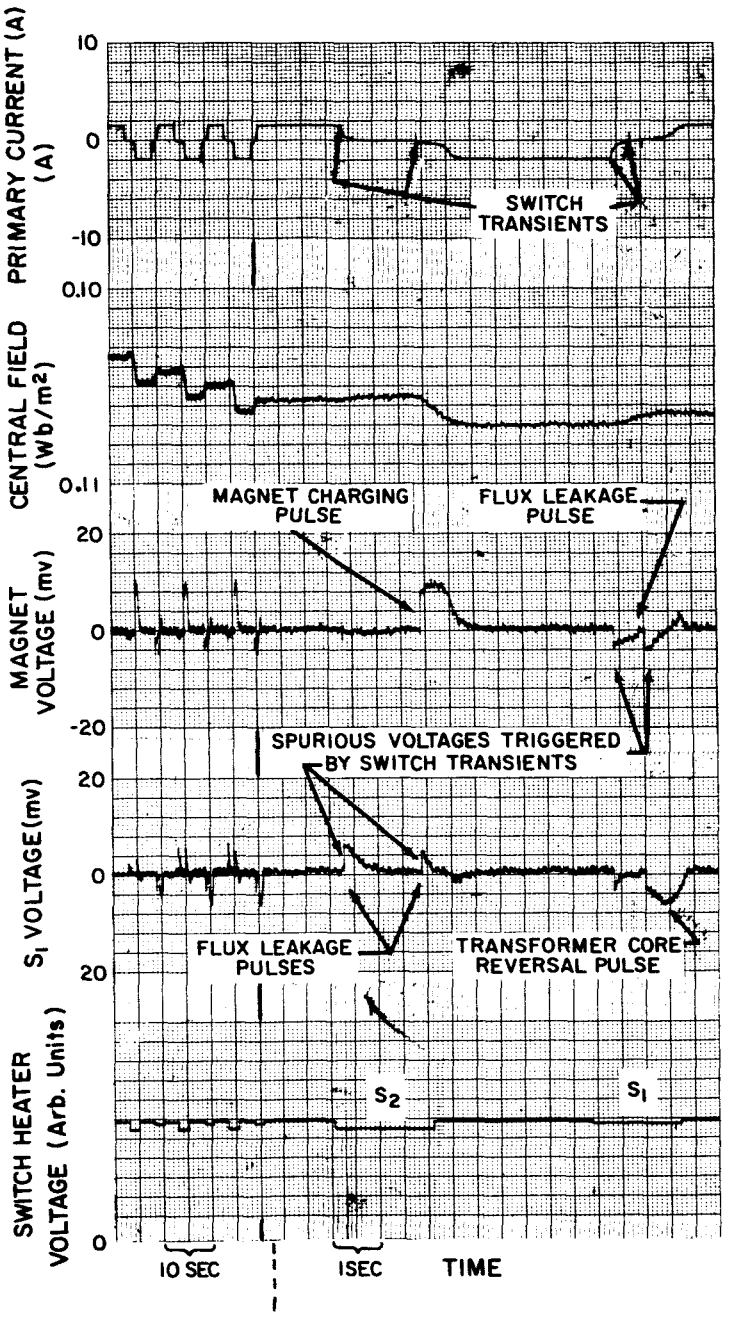

Fig. 31 Typical Time Dependance for Several Important Quantities Relating to the Operation of the Experimental Transformer Energizer. These are photographs of actual recordings taken during operation.

TABLE II

TRANSFORMER ENERGIZER TEST DATA

Total Charge Time, T_c	3300 sec.
Charge Cycle Time, T_N	7 sec.
Charge Pulse Time, T_p	1.4 sec.
Charge Pulse Time Fraction, τ_p	.14
Total Charge Cycles, N	450
Secondary Charge Voltage, V	8 mv
Maximum Field, B_o	.314 Wb/m^2
Maximum Current, I_L	542 A
Maximum Energy, E_s	734 Joules
Dimensionless Energy, β	.221
Maximum Heater Temp., Θ_D	10.5°K
Specific Boiloff, M	$1.25\ 10^{-2}$ liters/Joule
Channel 1	Transformer Primary Current
Channel 2	Central Field
Channel 3	Magnet Terminal Voltage
Channel 4	Voltage Across S_1
Channel 5	Switch Heater Voltage

2) While the core is being returned to its original state of negative saturation there should be no voltage pulses applied to the magnet because S_2 should remain superconducting during this time. Voltage pulses should be observed only across switch S_1 during this second half of the charge cycle. The fact that they do occur here shows that some of the flux is leaking back out each time and this is confirmed by the fact that the central magnetic field (Channel 2) can be seen to decay during this time.

3) The current in the primary is controlled by cam operated switches which cause small transients that can be seen in the Channel 1 primary current data. There is a definite time correlation between these transients and the appearance of the spurious magnet terminal voltage mentioned above. Evidently these transients cause normal regions to appear momentarily in the persistent switch S_2, allowing some of the flux to leak back out. Similar spurious voltages are seen to occur in S_1 during the charging part of the cycle, causing a flux leak there also.

As the magnet current increased the flux leak became more and more pronounced until at about 540 A the flux introduced each cycle, became equal to that leaking out so that no further gain could be realized.

4) There appears to be no correlation between the spurious voltages and the leading or trailing edges of the switch heater pulses.

5) Both the charging pulse and the core flux reversal pulse continue on after completion of the heater pulse. This confirms that sufficient heat is generated for "open" state operation without the help of the auxiliary heater once it is started. Since the major portion of the boiloff is due to the heaters, considerable gain in efficiency could be realized by applying very short heater pulses at the proper time.

The boiloff rate was measured during the operation of the flux pump and from this the specific boiloff was found to be $1.26\ 10^{-2}$ liters/Joule. It is useful to correlate this with the theory outlined in the preceeding section. This can be done with the help of an asymptotic approximation of the specific boiloff given in the theory. When the energy parameter, β, is less than unity, the temperature can be approximated by:

$$\phi \approx q$$

The specific boiloff can then be expressed approximately as:

$$M \approx \frac{2 E_s L}{\rho \ell \tau_p T_c \gamma_{He} C_L} \quad \frac{2q}{\beta}$$

Substitution for β then results in

$$M \approx \frac{4\sqrt{2}\, N \gamma_s C_s \Theta_c^{\,2} \ell_q}{3\, \gamma_{He} C_L \Theta_r J_c \sqrt{E_s L}} = 2.03\, 10^{-3} q$$

where

$$\gamma_s = 8.9 \text{ gm/cm}^3$$

$$C_s = .35 \text{ Joules/gm}^{\circ}\text{K}$$

$$\Theta_c = 6^{\circ}\text{K}$$

$$\ell = 180 \text{ cm}$$

$$\gamma_{He} = 125 \text{ gm/liter}$$

$$C_L = 21.6 \text{ Joules/gm}$$

$$\Theta_r = 300^{\circ}\text{K}$$

$$J_c = 5400 \text{ A/cm}^2$$

If this is compared to the actual measured boiloff it is found that

$$q = 3.08$$

$$\phi = \sqrt{q} = 1.75$$

$$\Theta_D = \phi \Theta_c = 10.5^{\circ}\text{K}$$

This value of q is quite reasonable for the geometry used. In these switches the entire length was heated so that $d \approx \ell$ and

$$q = \frac{3fd}{2\ell} \approx \frac{3}{2} f$$

The heat transfer efficiency factor f, would then need to be of the order of 2, which is quite reasonable since no account was taken for the heat leak out the switch leads.

The main object of the experiment was not to design an efficient operational unit but rather to design a highly instrumented model which could be used to check the theory outlined above and point out trouble spots for later development work. In this respect the unit was quite successful. In summary the following facts were revealed.

1) The theory outlined above has been confirmed.

2) The switches are subject to problems similar to those found in coils in that they are subject to unstable operation even when constructed from stabilized material. This stems from the conflicting requirements for the switch design. In order to insure efficient switch operation a minimum of liquid cooling is desired. Stable operation in the superconducting state, on the other hand, requires a maximum of liquid cooling capability. Some development work is therefore indicated in order to arrive at a satisfactory compromise.

REFERENCES

1. Avco Everett Research Laboratory, Annual Report on Contract NAS-8-5279, September 1964, p. 37, "Experimental Investigation of Advanced Superconducting Magnets," by Ethan Hoag.

2. Avco Everett Research Laboratory, Annual Report on Contract NAS-8-5279, July 1965, p. 11-18, "Experimental Investigation of Advanced Superconducting Magnets," by Ethan Hoag.

3. Avco Everett Research Laboratory, Annual Report on Contract NAS-8-5279, July 1965, p. 43, "Experimental Investigation of Advanced Superconducting Magnets," by Ethan Hoag.

4. Avco Everett Research Laboratory, Annual Report on Contract NAS-8-5279, July 1965, p. 47, "Experimental Investigation of Advanced Superconducting Magnets," by Ethan Hoag.

5. A.R. Kantrowitz and Z.J.J. Stekly, "A New Principle for the Construction of Stabilized Superconducting Coils," Appl. Phys. Letters 6, 56 (1965).

6. Brentari, E.G., Giarratano, P.T. and Smith, R.V., "Boiling Heat Transfer for Oxygen, Nitrogen, Hydrogen and Helium," NBS Technical Note No. 317, 1965.

7. Stekly, Z.J.J. and Zar, J.L., "Stable Superconducting Coils," Avco Everett Research Laboratory Research Report 210, 1965.

8. Rohsenow, W.M. and Choi, H.Y., "Heat, Mass and Momentum Transfer," Prentice Hall, 1961.

9. Sydoriak, S.G. and Roberts, T.R., Journal of Applied Physics, Vol. 28, No. 2, February 1957, p. 143.

10. H. Van Beelen, et al, Physica 31, 413.

11. I. Buckhold, Cryogenics, 4, 212 (1964).

12. H.L. Laquer, Cryogenics, 3, 27 (1963).

13. J. Volger and P.S. Admiral, Physics Letters, 2, 257 (1962).

14. S.L. Wipf, Advances in Cryogenic Engineering, 9, 345 (1963).

15. S. L. Wipf, Scientific Paper 65-1J9-LOTEM-P7, Westinghouse Electric Corp. (1965).

16. A. J. Volger, Advances in Cryogenic Engineering, 10B, 98 (1964).

17. J. E. C. Williams, Cryogenics, p. 234, December 1963.

18. Richard McFee, Rev. Sci. Inst., 30, 98 (1959).

19. Avco Everett Research Laboratory, Annual Report on Contract NAS-8-5279, July 1965, p. 47, "Experimental Investigation of Advanced Superconducting Magnets," by Ethan Hoag.